doi:10.1093/brain/awt250 Brain 2013: 136; 3305–3332 | 3305

BRAIN
A JOURNAL OF NEUROLOGY

Transcriptomic indices of fast and slow disease progression in two mouse models of amyotrophic lateral sclerosis

Giovanni Nardo,[1,3] Raffaele Iennaco,[1] Nicolò Fusi,[2] Paul R. Heath,[3] Marianna Marino,[1] Maria C. Trolese,[1] Laura Ferraiuolo,[3] Neil Lawrence,[2] Pamela J. Shaw[3,*] and Caterina Bendotti[1,*]

1 Laboratory of Molecular Neurobiology, Department of Neuroscience, IRCCS - Istituto di Ricerche Farmacologiche Mario Negri, Via La Masa, 19, 20156 Milan, Italy
2 Sheffield Institute for Translational Neuroscience, Department of Neuroscience, Computational Biology Unit, Faculty of Medicine, Dentistry and Health University of Sheffield 385A Glossop Road, Sheffield S10 2HQ, UK
3 Sheffield Institute for Translational Neuroscience, Department of Neuroscience, Academic Neurology Unit, Faculty of Medicine, Dentistry and Health University of Sheffield 385A Glossop Road, Sheffield S10 2HQ, UK

*These authors contributed equally to this work.

Correspondence to: Dr. Caterina Bendotti,
Laboratory of Molecular Neurobiology,
Department of Neuroscience,
IRCCS - Mario Negri Institute for Pharmacological Research,
Via La Masa,
19, 20156 Milan,
Italy
E-mail: caterina.bendotti@marionegri.it

Correspondence may also be addressed to: Professor Pamela J. Shaw, Department of Neuroscience, Academic Neurology Unit, Sheffield Institute for Translational Neuroscience (SITraN), University of Sheffield, 385A Glossop Road Sheffield S10 2HQ, UK, E-mail: pamela.shaw@sheffield.ac.uk

Amyotrophic lateral sclerosis is heterogeneous with high variability in the speed of progression even in cases with a defined genetic cause such as superoxide dismutase 1 (*SOD1*) mutations. We reported that *SOD1*^{G93A} mice on distinct genetic backgrounds (C57 and 129Sv) show consistent phenotypic differences in speed of disease progression and life-span that are not explained by differences in human *SOD1* transgene copy number or the burden of mutant SOD1 protein within the nervous system. We aimed to compare the gene expression profiles of motor neurons from these two *SOD1*^{G93A} mouse strains to discover the molecular mechanisms contributing to the distinct phenotypes and to identify factors underlying fast and slow disease progression. Lumbar spinal motor neurons from the two *SOD1*^{G93A} mouse strains were isolated by laser capture microdissection and transcriptome analysis was conducted at four stages of disease. We identified marked differences in the motor neuron transcriptome between the two mice strains at disease onset, with a dramatic reduction of gene expression in the rapidly progressive (129Sv-SOD1^{G93A}) compared with the slowly progressing mutant SOD1 mice (C57-SOD1^{G93A}) (1276 versus 346; *Q*-value $\leqslant$ 0.01). Gene ontology pathway analysis of the transcriptional profile from 129Sv-SOD1^{G93A} mice showed marked downregulation of specific pathways involved in mitochondrial function, as well as predicted deficiencies in protein degradation and axonal transport mechanisms. In contrast, the transcriptional profile from C57-SOD1^{G93A} mice with the more benign disease course, revealed strong gene enrichment relating to immune system processes compared with 129Sv-SOD1^{G93A} mice. Motor neurons from the more benign mutant strain demonstrated striking complement activation, over-expressing genes normally

Received April 30, 2013. Revised July 23, 2013. Accepted July 24, 2013. Advance Access publication September 24, 2013

involved in immune cell function. We validated through immunohistochemistry increased expression of the C3 complement subunit and major histocompatibility complex I within motor neurons. In addition, we demonstrated that motor neurons from the slowly progressing mice activate a series of genes with neuroprotective properties such as angiogenin and the nuclear factor (erythroid-derived 2)-like 2 transcriptional regulator. In contrast, the faster progressing mice show dramatically reduced expression at disease onset of cell pathways involved in neuroprotection. This study highlights a set of key gene and molecular pathway indices of fast or slow disease progression which may prove useful in identifying potential disease modifiers responsible for the heterogeneity of human amyotrophic lateral sclerosis and which may represent valid therapeutic targets for ameliorating the disease course in humans.

Keywords: amyotrophic lateral sclerosis; genetic background; immune system; motor neurons; SOD1

Abbreviations: ALS = amyotrophic lateral sclerosis; MHCI = major histocompatibility complex I; Ntg = non-transgenic; NRF2 = nuclear factor (erythroid-derived 2)-like 2; UCH37 = ubiquitin C-terminal hydrolase 37; PPLR = probability of positive log ratio

Introduction

Amyotrophic lateral sclerosis (ALS) is an irreversible adult onset neurodegenerative disorder that primarily causes injury and cell death of lower motor neurons in the brainstem and spinal cord, and upper motor neurons in the motor cortex (Cleveland and Rothstein, 2001; Peviani *et al.*, 2010; Ferraiuolo *et al.*, 2011). Progressive muscle denervation leads to spreading failure of the neuromuscular system resulting in death in most cases from respiratory failure within 2–3 years of symptom onset. The majority of ALS cases are sporadic whereas inherited forms account for up to 10% of cases. Twenty per cent of familial ALS is caused by mutation in the Cu/Zn superoxide dismutase (*SOD1*) gene. A body of evidence indicates that ALS is a heterogeneous disease with respect to the site and age of symptom onset and speed of disease progression (Beghi *et al.*, 2007). Although the disorder is invariably lethal, with a median survival of <5 years, 20% of patients survive >5 years and 10% of patients survive >10 years from symptom onset. This heterogeneity can be seen even in individual members of families with a common autosomal dominant mutation in SOD1. It is likely that such heterogeneity is due to specific molecular mechanisms that influence the course of the disease and the response to treatment.

Transgenic mice that overexpress various human SOD1 mutations replicate quite well multiple clinical and pathological features of human ALS (Gurney *et al.*, 1994; Bendotti and Carrì, 2004; Kato, 2008). These murine models develop severe and progressive motor neuron degeneration that leads to muscular weakness and paralysis culminating in death. As in the human disease, these mouse models may also vary in terms of age of onset, rapidity of disease progression, and certain histopathological features, mimicking the diversity of clinical phenotypes observed in human patients with ALS (Heiman-Patterson *et al.*, 2005, 2011). Such variability may be related to differences in specific SOD1 mutations, in the number of transgene copies or in the expression levels of the mutant SOD1 protein (Turner and Talbot, 2008). However, these animals show considerable variability in the onset and duration of the clinical features even among siblings, suggesting that there is genetic variability similar to the human disease in this rodent model that could be determined by potential disease modifying genes influencing specific biochemical pathways (Heiman-Patterson *et al.*, 2011).

Our understanding of disease pathogenesis has increased by the study of models of SOD1-related ALS and it is clear that multiple mechanisms contribute to motor neuron injury, including mitochondrial dysfunction, oxidative stress, protein misfolding/aggregation and axonal transport defects (Peviani *et al.*, 2010; Ferraiuolo *et al.*, 2011). In addition, it has become clear that certain aspects of ALS are non-cell autonomous and that other cell types within the CNS and periphery contribute to motor neuron injury including microglia, astrocytes, oligodendrocytes, macrophages and T cells (Boillee *et al.*, 2006*b*; Lobsiger and Cleveland, 2007; Appel *et al.*, 2010; Robberecht and Philips, 2013). Large scale microarray analysis represents an excellent tool to analyse the complex pathobiology of ALS and to elucidate the contribution of specific biochemical pathways to the neurodegenerative process (Cooper-Knock *et al.*, 2012). Furthermore, with the development of technology for isolating individual cells using laser capture microdissection, it has now been possible to analyse, on a genome-wide level, molecular changes in specific cell types, reducing the background noise arising from whole tissue analysis.

Several studies have combined laser capture microdissection and microarray analysis in the spinal cord of transgenic mice as a means for identifying pathophysiological changes that occur in motor neurons during disease progression in ALS (Perrin *et al.*, 2005, 2006; Ferraiuolo *et al.*, 2007; Lobsiger *et al.*, 2007; Saxena *et al.*, 2009). These studies principally focused on a comparison of mice with the same genetic background but different SOD1-related mutations with the aim of identifying common gene alterations in different ALS mice models as biomarkers of the disease. Key transcripts and pathways which were differentially expressed at different stages of the disease course have been identified in these reports. However, no previous gene expression analysis has attempted to analyse the effects of the genetic background on the phenotype of the murine disease, which may represent an important means of identifying factors influencing the rate of disease progression.

Recently, Mancuso *et al.* (2012) reported differences in disease onset and progression between C56BL/6 and B6SJL mouse strains carrying the same number of copies of the mutant G93A human

SOD1 transgene. Heiman-Patterson *et al.* (2011) have also examined the effects of different genetic backgrounds on the phenotype of SOD1^{G93A} mice. Preliminary results from an ongoing study showed that the SOD1^{G93A}-NOD.RAG1KO line, which lack a functional immune system, showed a more aggressive disease course, suggesting a protective role of neuroinflammation, despite years of conjecture that inflammation is a major contributor to motor neuron injury (Ende *et al.*, 2000; Yi *et al.*, 2000; Glass *et al.*, 2010; Papadimitriou *et al.*, 2010). These reports highlight the importance of the genetic background on disease progression.

We previously reported that 129Sv mice show a much faster disease progression, with survival of 129 ± 5 days compared to a survival of 180 ± 16 days for the C57 mouse strain, even though they carry the same copy numbers of the human mutant SOD1 transgene and express the same amount of mutant SOD1 protein in the spinal cord (Pizzasegola *et al.*, 2009). In the present study we combined laser capture microdissection and whole genome transcriptome analysis to identify alterations in the gene signature within motor neurons isolated from the lumbar spinal cord from C57-SOD1^{G93A} (slowly progressing) mice and 129Sv-SOD1^{G93A} (rapidly progressing) mice at different stages of the disease course.

We identified a marked difference in the motor neuron gene signature between the two mouse strains at the onset of the disease, before the appearance of overt signs of muscle weakness. At this stage of disease onset, motor neurons from the rapid progressor strain exhibit a marked impairment of specific pathways principally involved in mitochondrial function, protein degradation pathways and protein targeting, whereas the transcriptional profile of motor neurons from the slow progressor strain revealed an upregulation of genes involved in inflammation and immune system regulation such as major histocompatibility complex I (*MhcI*), chemokine (C-C motif) ligand 12 (*Ccl12*), complement component 3 (*C3*), coupled with a stable expression of key neuroprotective factors such as angiogenin (*Ang*) and nuclear factor (erythroid-derived 2)-like 2 (*Nrf2*, now known as *Nfe2l2*). These results indicate that genetic background has a major influence on the lifespan of SOD1 mutant mice. It is noteworthy that biological processes like an early inflammatory response, classically considered detrimental, appear to slow down disease progression. The interactions of mutant SOD1 with specific genetic modifiers and pathways, which vary in expression in different strains of mice, may be helpful in identifying therapeutic targets for ameliorating disease progression in human ALS.

Materials and methods

Mouse models

Mice were maintained at a temperature of 21 ± 1°C with a relative humidity 55 ± 10% and 12 h of light/dark cycle. Food (standard pellets) and water were supplied *ad libitum*. Procedures involving animals and their care were conducted according to the Mario Negri institutional guidelines, that are in compliance with national (D.L. no. 116, G.U. suppl. 40, Feb.18, 1992, Circular No.8, G.U., 14 luglio 1994) and five international laws and policies (EEC Council Directive 86/609, OJ L 358, 1 Dec.12, 1987; NIH Guide for the Care and use of Laboratory Animals, U.S. National Research Council, 1996). All the experiments and the protocol proposed in the project were examined first by the Institutional Ethical Committee and then sent to the Italian Ministry of Health for authorization. The mice were bred and maintained in a specific pathogen-free environment. Animals with substantial motor impairment had food on the cage bottom and water bottles with long drinking spouts.

Female transgenic SOD1^{G93A} mice of C57BL/6JOlaHsd (C57-SOD1^{G93A}) or 129SvHsd (129Sv-SOD1^{G93A}) genetic background and corresponding non-transgenic female littermates were used in this study. Both mouse lines derive from the line originally obtained from Jackson Laboratories (B6SJL-TgNSOD-1-SOD1G93A-1Gur) expressing ~20 copies of human mutant SOD1 with a Gly93Ala substitution and were maintained on a C57OlaHsd or 129SvHsd background (for more than 30 or 10 generations, respectively) at Harlan Italy S.R.L. The two transgenic mouse strains show major clinical differences in terms of age of symptom onset, survival length and disease duration (Pizzasegola *et al.*, 2009). Analysis of motor dysfunction was performed as reported in Pizzasegola *et al.* (2009). The onset of symptoms was considered when the mice showed the first sign of impairment on paw grip strength and the body weight started to decline. The symptomatic and the end stages were considered when the mice exhibited a decrease of ~50% or ~80%, respectively, in their latency on the grip strength and the body weight declined >5% or 20%, respectively, from the initial value.

Microarray analysis: tissue preparation

Spinal cord tissues were obtained from C57 and 129Sv transgenic SOD1^{G93A} mice and age-matched non-transgenic littermates at the presymptomatic, the early symptomatic (onset) stage, symptomatic and end stage corresponding to initial, 50% or 80% impairment of grip strength. Mice at the different disease stages were intracardially perfused with 30% sucrose solution and the spinal cords were removed, the lumbar segment dissected out and included in OCT™ compound (Tissue-Tek®) before snap freezing and storage at −80°C until required. Frozen tissue sections (8 µm) were cut in a cryostat at −22°C, thaw mounted onto slides at room temperature, fixed in 70% ethanol, washed in diethylpyrocarbonate-treated water, and stained for 30 s in a solution of 0.1% w/v toluidine blue in 0.1 M sodium phosphate. Sections were then washed and dehydrated through graded ethanol concentrations (70%, 90% and 100%), and xylene (two washes of 5 min). Spinal motor neurons, identified by staining, anatomical location, size and morphology, were isolated on Arcturus Capsure Macro laser capture microdissection caps using the Veritas 704 Laser Capture Microdissection System (Harlow Scientific). Approximately 1000 motor neurons were dissected from the lumbar spinal cord of each mouse.

RNA amplification and microarray hybridization

RNA was extracted and purified from each sample using the PicoPure™ RNA isolation kit (Applied Biosystems), and amplified using the antisense RNA one cycle amplification process with GeneChip® 3′ IVT Express Kit (Affymetrix). This process is considered the gold standard preparation for gene expression analysis. Reverse transcription-*in vitro* transcription was experimentally validated using TaqMan® RT-PCR (MAQC Consortium *et. al*, 2006). Sixteen chips (four C57-SOD1^{G93A} versus four C57-Ntg and four 129Sv-SOD1^{G93A} versus four 129Sv-Ntg) were hybridized at each of the four time points according to the Affymetrix protocol. Amplified

complementary RNA (15 μg) for each sample was fragmented and hybridized to GeneChip Mouse Genome 430 2.0 (Affymetrix) and scanned in the GeneChip Scanner 3000 for quantification of the hybridization signal.

Microarray data analysis

CEL files generated by the Affymetrix GeneChip Operating System were analysed using the probabilistic model implemented in the bioconductor package PUMA (Gentleman *et al.*, 2004; Rattray *et al.*, 2006; Pearson *et al*., 2009). This model combines the uncertainty estimates from replicated experiments in order to obtain point estimates and standard errors of the expression levels within each condition. Compared to the traditional statistical approach, which does not incorporate this information, this modelling approach results in a more robust and accurate analysis of differential gene expression (Liu *et al.*, 2006). For each gene, the model returns the probability of positive log ratio (PPLR), which is then transformed in a Q-value (Storey, 2006) in order to account for multiple hypotheses testing. The data discussed in this publication have been deposited in NCBI's Gene Expression Omnibus (Edgar *et al*., 2002) and are accessible through GEO Series accession number GSE46298.

Systems biology analysis

The Database for Annotation, Visualization and Integrated Discovery (DAVID) (http://david.abcc.ncifcrf.gov/) and the commercial software Metacore™ (http://www.genego.com/metacore.php) were used to perform the systems biology analysis of the differentially expressed genes. DAVID is a web-based tool that provides integrated solutions for the annotation and analysis of genome-scale data sets derived from high-throughput technologies. MetaCore™ is an integrated knowledge database and software suite for pathway analysis of experimental data and gene lists. MetaCore™ is based on a proprietary manually curated database of human protein–protein, protein–DNA and protein compound interactions, metabolic and signalling pathways for human, mouse and rat, supported by proprietary ontologies and controlled vocabulary. Both DAVID and MetaCore™ categorize gene identities by Gene Ontology (GO) annotation (http://www.geneontology.org/), which classifies transcripts according to their molecular function, biological process and cellular component. The statistical significance of each functional enriched cluster and pathway is indicated in both DAVID and Metacore™ by a *P*-value yielded from Fisher's exact test.

The GeneGo analysis of GO Cellular Process (Metacore™) defines a statistical classification of the main biological processes on the basis of the identity of transcripts with altered expression as well as through their potential interactions within annotated biological networks. Gene IDs of the data set(s) of interest are mapped to gene IDs in entities (terms) of built-in functional ontologies represented in Metacore™ by pathway maps and networks. The mapping procedure involves calculating the statistical relevance of the matches found. Both private GeneGo and public GO ontologies (GO processes, GO molecular function, GO localization) are used for the analysis. The statistical relevance of the ontology matches found is calculated as a *P*-value directly proportional to the number of processes related to the active data set. The lower the *P*-value, the higher is the 'non-randomness' of finding the intersection between the data set and the particular ontology. Canonical pathway maps represent a set of comprehensive signalling and metabolic maps. All maps are created by Thomson Reuters scientists by a high-quality manual curation process based on published peer-reviewed literature.

Immunoblotting techniques

Mice were sacrificed according to institutional ethical procedures by decapitation and the spinal cord was removed without fixation. The samples were immediately frozen on dry ice with the ventral portion of spinal cord face-up and stored at −80°C. For each mouse, lumbar spinal cord was longitudinally transected in 50 μm cryostat ventral and dorsal spinal cord sections as separate samples. The resulting cryostat ventral material was homogenized by sonication in ice-cold homogenization buffer (20 mM Tris-HCl pH 7.4, 2% Triton™ X-100, 150 mM NaCl, 1 mM EDTA, 5 mM $MgCl_2$, 1 mM phenylmethylsulphonyl fluoride, and protease inhibitor cocktail, Roche), centrifuged at 13 000 rpm for 30 min at 4°C and the supernatants were collected and stored at −80°C. Equal amounts of total protein homogenates were loaded on polyacrylamide gels and electroblotted onto PVDF (Millipore) membrane as previously described (Basso *et al.*, 2009). Alternatively, protein extracts were directly loaded on nitrocellulose membrane, Trans-Blot® Transfer Medium (Bio-Rad), by vacuum deposition on the Bio-Dot® SF blotting apparatus (Bio-Rad) as previously described (Nardo *et al.*, 2009, 2011). Membranes were immunoblotted with the following primary antibodies: rabbit polyclonal anti-ANG (1:1000; Abcam); rabbit polyclonal anti-ATF-3 (1:1000; SantaCruz); rabbit polyclonal anti C3 H300 (1:100; Santa Cruz); rabbit polyclonal anti-KIF 5 A + B + C (1:1000; Abcam); rabbit polyclonal anti-NRF2 (1:200; Santa Cruz); rabbit monoclonal anti-UCH37 (1:1000; Abcam) mouse anti-β-actin (1:30000; Chemicon) followed by horseradish peroxidase-conjugated secondary antibodies (Santa Cruz) and developed by Luminata™ Forte Western Chemiluminescent HRP Substrate (Millipore) on the ChemiDoc™ XRS system (Bio-Rad). Densitometry was determined with Progenesis PG240 v2006 software (Nonlinear Dynamics). Immunoreactivity was normalized to β-actin or alternatively to the actual amount of proteins loaded on the membrane, as detected after Red Ponceau staining (Fluka). The immunoblotting analysis was performed for each protein on the ventral portion of lumbar spinal cord from four C57-SOD1^{G93A} and four 129-SOD1^{G93A} mice at the symptom onset stage and four age-matched non-transgenic mice for each strain. Statistical comparisons between groups were performed through two-way ANOVA using the Tukey's *post hoc* test for multiple comparisons.

Immunohistochemistry

Anaesthetized mice were perfused transcardially with 4% paraformaldehyde and spinal cord dissected, post-fixed in 4% paraformaldehyde overnight at 4°C, preserved in 30% sucrose and then included in OCT™ compound. Immunohistochemical analyses were performed on free floating spinal cord cryosections (30 μm) and, after mounting on glass slides (Walderlmar Knittle) with 1:1 0.1 M PBS: glycerol, fluorescence-labelled samples were analysed under an Olympus Fluoview laser scanning confocal microscope (Olympus BX61 light microscope).

For immunohistochemical analysis of major histocompatability class I (MHCI) an alternative fixative procedure was performed according to the method described by Thams *et al.* (2009). Briefly, mice were perfused with Tyrodes's buffer, followed by Lana's fixative (4% formalin and 0.4% picric acid in 0.16 M PBS, pH 7.2) at 20°C. The lumbar spinal cord, sciatic nerve, and gastrocnemius muscles were quickly dissected out. The tissue was left in the same fixative for 90–180 min or overnight at 4°C, rinsed, and stored for 24 h in 10% sucrose with 0.1% sodium azide in 0.01 M PSB at 4°C for cryoprotection, before mounting in OCT™ compound. The spinal cords, sciatic nerves, and muscles were cut as 30, 14, and 20 μm sections, respectively. Spinal cord immunohistochemistry was performed on

free-floating sections while nerve and muscle preparations were treated directly on gelatinized objective slides.

The following primary antibodies were used: rabbit polyclonal anti-ANG (1:1000; Santa Cruz); rabbit polyclonal anti-NRF2 (1:200; Santa Cruz); rabbit polyclonal anti-ATF-3 (1:500; Santa Cruz); rabbit monoclonal anti-UCH37 (1:200; Abcam); rabbit polyclonal anti-KIF 5 A + B + C (1:500; Abcam); rat monoclonal anti-MHC class I ER-HR 52 clone (1:100; Abcam), rat anti-C3b/iC3b/c3c (1:50; Hycult Biotech), rabbit anti-C3 H300 (1:100; Santa Cruz), mouse anti-SMI-31 (1:500; Sternberger Inc), rabbit anti-GFP (1:1000; Molecular Probes), rabbit anti-synaptophysin (1:200; Sigma Aldrich), isolectin GS-IB4 Alexa Fluor® 488 conjugate (1:200; Sigma), α-btx (5μg/ml) conjugated with Alexa Fluor® 594 (Invitrogen), neurotrace conjugated with Alexa Fluor® 488 or Alexa Fluor® 594 (Invitrogen), mouse anti-GFAP (1:2500; Millipore); mouse anti-CNPase (1:100; Millipore). Secondary antibodies were as follows: Alexa Fluor® 488 or Alexa Fluor® 594 goat anti-rat, Alexa Fluor® 488 or Alexa Fluor® 594 goat anti-rabbit, Alexa Fluor® 594 goat anti-mouse (Invitrogen). All the immunohistochemistry was performed through an indirect immunostaining protocol apart from ATF-3 for which an immunoperoxidase procedure was used. Briefly, tissue sections were treated with 1% hydrogen peroxide in PBS to inhibit endogenous peroxidases, blocked in 1% bovine serum albumin in PBS containing 0.2% Triton™ X-100 for 30 min and then incubated overnight with the primary antibodies diluted in PBS containing 0.1% bovine serum albumin. Immune reactions were revealed by 60 min incubation in the appropriate secondary biotinylated antiserum goat anti-rabbit (Vector Laboratories), followed by 75 min incubation in the avidin-biotin-peroxidase complex (Sigma) and using diaminobenzidine as the chromogen. Immunohistochemistry with monoclonal antibody to mouse C3b/iC3b/c3c and CNPase was performed with the Cy5-Tyramide Signal Amplification (TSA) system (Perkin Elmer, Inc). For each approach, control sections processed with omission of the primary antiserum and developed under the same conditions gave no immunostaining.

The colorimetric histochemical assay for activities of the mitochondrial electron transport chain complexes was performed according to the protocol described by Jung *et al*. (2002*a*, *b*). This approach is based on an *in situ* enzyme-histochemical assay that allows quantification of the activity of the electronic transport chain protein complexes directly on unfixed cryostat sections of a selected CNS area. We analysed the activity of the complex I. In brief, fresh isolated lumbar spinal cords were embedded in OCT™ compound on dry ice and stored at −80°C until sectioning. Eight-micrometer sections were cut at −20°C and mounted on SuperFrost® Plus microscope slides (VWR). To measure complex I activity, sections were incubated in 0.1 M Tris-HCl, 0.1 mg/ml NADH, 1.0 mg/ml NBT, 2 μg/ml antimycin A, 84 mM malonate and 2 mM KCN, pH 7.4 for 20 min. Photomicrographed immune-stained spinal cord sections ($n = 3$) from each mouse (three mice per group) were acquired using AnaliSYS software (SoftImaging Systems, ver. 3.2), imported in Fiji (ImageJ, Media Cybernatics) and assessed using quantitative densitometric analysis. A constant ventral horn size in each section was captured, the total number of pixels within that area was isolated, and the percentage of pixels darker than background was determined for each section after segmentation (area fraction). Statistical comparisons between groups was performed through two-way ANOVA using the Tukey's *post hoc* test for multiple comparisons.

ATP colorimetric assay

Tissue samples were processed as for the immunoblotting. The ATP colorimetric assay (BioVision) was performed according to the manufacturer's recommendations. ATP concentration (nmol/mg of tissue) was analysed in the ventral portion of lumbar spinal cord from four C57-SOD1^{G93A}, four 129-SOD1^{G93A} mice at the symptom onset and four age-matched non-transgenic mice for each strain. Statistical comparisons between groups was performed through two-way ANOVA using the Tukey's *post hoc* test for multiple comparisons.

In vitro experiments

Primary spinal neurons were prepared from spinal cord of 14-day-old C57-SOD1^{G93A} or non-transgenic mouse embryos. Cells were plated into wells previously coated with a layer of confluent non-transgenic astrocytes, cultured at 37°C in a humidified atmosphere of 95% air and 5% CO_2. After 5–6 days *in vitro*, cells were fixed with Lana's fixative for 30 min, and then processed for immunocytochemistry.

Results

Microarray analysis

The transcription profiles of laser captured motor neurons isolated from the lumbar ventral spinal cords of the rapid progressor (129Sv-SOD1^{G93A}), slow progressor (C57-SOD1^{G93A}) mice at four stages of the disease (presymptomatic, onset, symptomatic, end stage) (Supplementary Table 1) and respective non-transgenic littermates were generated using the murine GeneChip Mouse Genome 430 2.0 Plus (Affy MOE4302). To identify genes differentially expressed, CEL files generated by the Affymetrix GeneChip Operating System were analysed using the probabilistic model implemented in the Bioconductor package PUMA. Independent data outputs were produced at each stage of the disease for both mouse strains through the comparison of the gene expression profiles between four transgenic mice and four non-transgenic littermates. Probe sets with a Q-value $\leqslant 0.01$ and a fold change $\geqslant 1.5$ were defined as significantly differentially expressed.

Gene expression profiles

Overall gene expression profiles for both the rapid and slow progressor strains compared to their relative non-transgenic littermates during the progression of the disease are shown in Fig. 1. Area-proportional Venn diagrams, summarizing gene identifiers overlapping between 129Sv and C57 transgenic mice at the four stages of the disease are shown in Supplementary Fig. 1. At the presymptomatic and symptomatic stages, the C57 and 129Sv transgenic mice show a comparable trend in the transcriptome profile, although motor neurons from the rapid progressor strain exhibit an increase in the number of downregulated genes compared with the slow progressor strain (presymptomatic: 17% versus 11%; symptomatic: 53% versus 46%). The end stage disease is characterized by a large increase in the number of transcripts with altered expression in the motor neurons from both strains, (C57-SOD1^{G93A}: 2716; 129Sv-SOD1^{G93A}: 4063), most of which are downregulated (C57-SOD1^{G93A}: 73% of the total; 129Sv-SOD1^{G93A}: 72% of the total) (Fig. 1). The motor neuron gene signature at disease onset best discriminates the two

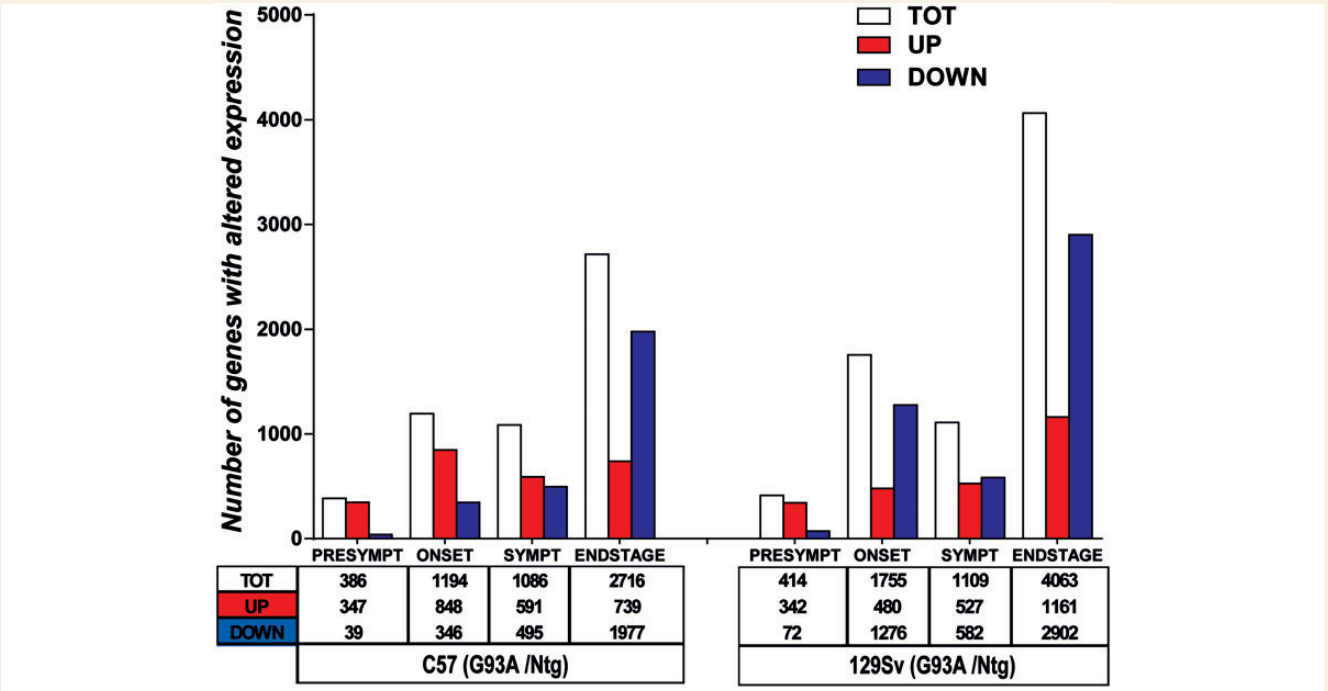

Figure 1 Gene expression profiles of C57-SOD1^{G93A} and 129Sv-SOD1^{G93A} motor neurons during the progression of the disease. The histograms (and corresponding tables) tabulate the distribution of genes with altered expression in motor neurons from both transgenic mice strains at the presymptomatic, onset, symptomatic and end stage. For each mouse strain the relative gene expression ratio [mean fold-change ratio between four SOD1^{G93A} and four non-transgenic (Ntg) mice; *Q*-value $\leqslant$ 0.01 and fold change $\geqslant$ 1.5] was obtained at each stage. White bars = total number of genes with altered expression; red bars = upregulated genes; blue bars = downregulated genes.

transgenic mouse strains. At the onset of the disease there is a dramatic downregulation of gene expression/transcriptional repression in the 129Sv-SOD1^{G93A} versus the C57-SOD1^{G93A} mice: (1276 versus 346 genes). In contrast, an increase in the number of upregulated genes characterizes the C57-SOD1^{G93A} compared with the 129Sv-SOD1^{G93A} strain (848 versus 480 genes) (Fig 1). It is striking that, of the 1101 genes specifically altered in 129Sv-SOD1^{G93A} motor neurons during this stage, 1055 (96%) are downregulated whereas of the 540 genes specifically altered in C57-SOD1^{G93A} motor neurons, 457 (85%) are upregulated (Fig. 2A). On the basis of these initial results, a more detailed analysis has been performed on the differentially expressed genes of the two strains of transgenic mice at the onset of the disease, with the aim of identifying specific molecular mechanisms and key gene modifiers that are associated with the difference in phenotype between the two mouse strains.

Systems biology analysis on genes differentially expressed between motor stage neurons from the fast and slow progressor mouse strains at disease onset

The GeneGo comparative analysis (Metacore^{TM}) performed on the whole list of genes with altered expression from both transgenic mice at the onset of the disease (C57-SOD1^{G93A}: 1194 genes; 129Sv-SOD1^{G93A}: 1755 genes) identifies a greater number of active biological processes in C57-SOD1^{G93A} motor neurons versus 129Sv-SOD1^{G93A} motor neurons, which relate to the stress response (Supplementary Fig. 2). The GO categories, deriving from the 'response to stress' category (GO: 0006950), are apparent in the transcriptome profile of both transgenic mice ['defence response' (GO: 0006952 *P*-value: 1.27×10^{-44}); 'response to stimulus' (GO: 0050896 *P*-value: 1.59×10^{-37}); 'response to wounding' (GO: 0009611 *P*-value: 9.11×10^{-34})]. However, for each of these categories, a large number of processes are specifically activated in the C57-SOD1^{G93A} motor neurons ('defence response': 37; 'response to wounding': 37; 'response to stimulus': 29) (Supplementary Fig. 2).

Interestingly, GO biological processes underlying the ancestral category 'regulation of immune system' ['immune system process' (GO: 0002376 *P*-value: 1.21×10^{-39}); 'immune response' (GO: 0006955 *P*-value: 3.17×10^{-46}); 'regulation of immune system process' (GO: 0002682 *P*-value: 1.2×10^{-32})] are significantly related to the motor neuron transcriptome of both transgenic mice (Supplementary Fig. 2). Again a higher number of biological processes are specifically linked to C57-SOD1^{G93A} and not to 129Sv-SOD1^{G93A} motor neurons. Thirty-six, 24 and 21 biological processes related to the 'immune system process', the 'immune response' and the 'regulation of immune system process', respectively are exclusively upregulated in C57-SOD1^{G93A} motor neurons at disease onset.

To better discriminate the two transgenic mice strains, we independently analysed in DAVID the lists of transcripts specifically altered in C57-SOD1^{G93A} (540 genes) and 129Sv-SOD1^{G93A} (1101 genes) motor neurons at the onset of the disease (Fig. 2A).

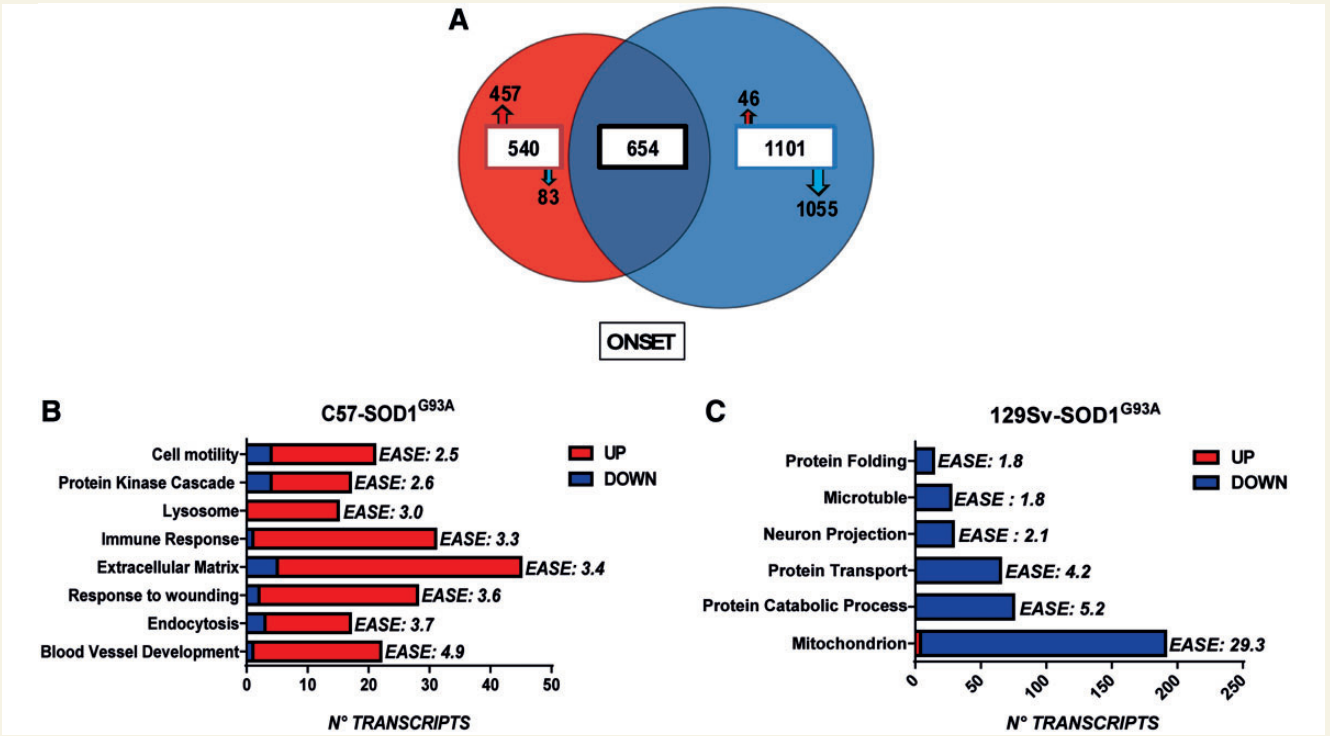

Figure 2 Gene distribution and enrichment analysis of C57-SOD1^{G93A} and 129Sv-SOD1^{G93A} motor neurons at disease onset. (**A**) Area proportional Venn diagram, summarizing gene identifiers overlapping (654 genes) between motor neurons from 129Sv-SOD1^{G93A} (blue) and C57-SOD1^{G93A} (red) mice at disease onset. The analysis of gene distribution shows the specific alteration of 540 genes in C57-SOD1^{G93A} motor neurons, 457 of which are upregulated (red arrow) and 83 downregulated (blue arrow). 129Sv-SOD1^{G93A} motor neurons show the specific alteration of 1101 genes, 46 of which are upregulated (red arrow) and 1055 downregulated (blue arrow). (**B** and **C**) DAVID enrichment analysis performed on transcripts specifically altered in C57-SOD1^{G93A} motor neurons (n = 540 genes) and 129Sv-SOD1^{G93A} motor neurons (n = 1101) at disease onset, identifies the most significant upregulated biological processes and the most significant downregulated biological processes in C57-SOD1^{G93A} and 129Sv-SOD1^{G93A} motor neurons, respectively. The significance of each gene cluster is evaluated through the enrichment score (EASE). An EASE $\geqslant$ 1.8 is equivalent to a non $-$log scale of 0.01.

We performed functional annotation clustering (DAVID) to classify the principal enriched biological functions in C57-SOD1^{G93A} and 129Sv-SOD1^{G93A} motor neurons. This approach allows ranking of the biological importance of the annotation terms (GO annotations) on the basis of the degree of their co-association with differentially expressed genes (gene IDs), assigning an enrichment score (EASE) that represents a modified Fisher exact P-value, for gene-enrichment analysis (Huang *et al.*, 2009). We selected as significant only functional gene clusters with an EASE $\geqslant$1.8 (equivalent to a non $-$log scale of 0.01). This allowed us to identify the main biological processes linked to the specific gene signature of motor neurons from the rapid and slow progressor mouse strains, respectively at disease onset (Fig. 2B and C).

Upregulated pathways in C57-SOD1^{G93A} motor neurons at disease onset

Immune system processes in C57 motor neurons

The analysis of the 'cytokine–cytokine receptor interaction' Kyoto Encyclopedia of Genes and Genomes (KEGG) pathway, that accounts for 38 transcripts of C57-SOD1^{G93A} motor neurons (P-value: 3.3×10^{-6}) and 33 transcripts of 129Sv-SOD1^{G93A} motor neurons (P-value: 9.5×10^{-2}) (Supplementary Fig. 3A and B; Supplementary Table 2), reveals a more prominent immune reactivity/modulation in motor neurons from the slow progressor mouse strain. In particular, C57-SOD1^{G93A} motor neurons show a higher upregulation of transcripts coding for monocyte/T cells chemoattractant proteins such as *Ccl12* (*Mcp-5* or MCP-1 related protein) (129Sv-SOD1^{G93A} fold change = 2.5; C57-SOD1^{G93A} fold change = 10.4), chemokine (C-X-C motif) ligand 10 (129Sv-SOD1^{G93A} fold change = 5.6; C57-SOD1^{G93A} fold change = 13.9), chemokine (C-X-C motif) ligand 16 (129Sv-SOD1^{G93A} fold change = 2.8; C57-SOD1^{G93A} fold change = 6.0) and chemokine (C-C motif) ligand 5 (129Sv-SOD1^{G93A} fold change = $-$1.2; C57 fold change = 8.6) whereas 129Sv motor neurons exhibit a stronger upregulation of cardiotrophin-like cytokine factor 1 (129Sv-SOD1^{G93A} fold change = 5.3; C57-SOD1^{G93A} fold change = 3.4) and chemokine (C-X-C motif) ligand 13, (129Sv-SOD1^{G93A} fold change = 125.8; C57-SOD1^{G93A} fold change = 5.2) involved in maturation and recruitment of B cells, respectively (Senaldi *et al.*, 1999; Krumbholz *et al.*, 2006). In addition, C57-SOD1^{G93A} motor neurons exhibit a greater upregulation of different receptors for specific cytokines involved in inflammatory (interleukin 6 receptor alpha; Fas-TNF receptor superfamily

member 6; tumour necrosis factor receptor superfamily member 1a and 1b) as well as anti-inflammatory/neuroprotective (colony stimulating factor 1 receptor; colony stimulating factor 2 receptor beta; interleukin 2 receptor gamma chain; transforming growth factor beta receptor I and II; interleukin 10 receptor beta) processes.

The systems biology analysis performed through Metacore™ reveals oncostatin M signalling through JAK-STAT as the most significant cytokine-related 'canonical pathway' activated in both transgenic mouse strains at the stage of disease onset (Supplementary Fig. 4). This system is specifically inhibited by the suppressor of cytokines 3 (*Socs3*), which is more upregulated in 129Sv-SOD1^{G93A} (fold change = 9.2) than in C57-SOD1^{G93A} (fold change = 5.7) mice. Consistently, oncostatin M receptor (*Osmr*) shows a higher expression in C57-SOD1^{G93A} (fold change = 7.2) versus 129Sv-SOD1^{G93A} (fold change = 3.2) motor neurons. Motor neurons from both strains upregulate signal transducer and activator of transcription 3 (*Stat3*) with a fold change = 2.0 whereas only C57-SOD1^{G93A} motor neurons upregulate signal transducer and activator of transcription 1 (*Stat1*; fold change = 1.6). The activity of oncostatin M on motor neurons influences the expression pattern of the serine protease inhibitor A3N (*Serpina3n*), tissue inhibitor of metalloproteases 1 (*Timp1*) and *Mcp-5* that are all more upregulated in the C57-SOD1^{G93A} motor neurons (Fig. 3 and Table 1).

Complement pathway

Functional annotation clustering performed on 540 genes specifically altered in C57-SOD1^{G93A} motor neurons at disease onset identified eight gene clusters with EASE >1.8 (Fig. 2B). Amongst these the 'immune response' gene cluster (GO: 0006955) represents one of the most significantly upregulated biological processes (EASE: 3.3), with 32 immune transcripts specifically altered in C57-SOD1^{G93A} motor neurons (Supplementary Table 3). In particular, several subunits related to the complement pathway such as complement component 3 (*C3*) and complement component factor H (*Cfh*) are upregulated. In line with these observations, the analysis of the 'canonical pathways' (Metacore™) identifies the 'classical complement pathway' more significantly related to the C57-SOD1^{G93A} compared with the 129Sv-SOD1^{G93A} gene data set (Supplementary Fig. 4). C57-SOD1^{G93A} motor neurons strongly upregulate complement components such as *C3* and complement component 4B (*C4b*) (Fig. 4A; Supplementary Fig. 5 and Supplementary Table 4), but appear to finely regulate complement activation at different levels through the specific upregulation of C1-inhibitor (*Serping1*, fold change = 3.3) and *Cfh* (fold change = 1.9). C1-inhibitor forms a proteolytically inactive stoichiometric complex with the *C1r* or *C1s* proteases whereas *Cfh* functions as a cofactor in the inactivation of *C3b* by factor I and also increases the rate of dissociation of the C3 convertase and the (C3b)NBB complex (C5 convertase) in the alternative complement pathway (Rus *et al.*, 2005).

The specific upregulation of messenger RNA for *C3* in C57-SOD1^{G93A} motor neurons implies an increase in the expression of the *C3* subunit and activated *C3* downstream components (*C3a*, *C3b*, *C3ib*, *C3c*, *C3dg*). We confirmed this at protein level by immunohistochemical analysis of the lumbar spinal cord from both transgenic and age-matched control animals which demonstrate greater levels of *C3* and *C3* activated by-products in C57-SOD1^{G93A} compared to 129Sv-SOD1^{G93A} motor neurons (Fig. 4B and D). The increase of *C3* in C57-SOD1^{G93A} motor neurons was further validated through immunoblot analysis of enriched motor neuron fractions (longitudinal dissected ventral horns) from both transgenic mouse strains and their non-transgenic littermates (Fig. 4C).

Major histocompatibility complex I

The microarray data show that C57-SOD1^{G93A} motor neurons display more pronounced upregulation messenger RNAs encoding multiple surface antigens normally exposed on the cell membranes of haematopoietic stem cells and/or mature leucocytes and monocytes (*Cd22*; *Cd86*; *Cd44*; *Ncam1*) (Supplementary Table 5). Most importantly, motor neurons for the slow progressing mouse strain specifically overexpress different class Ia components of the MHCI (Supplementary Table 3) and also show greater levels of beta-2 microglobulin (*β2m*; 129Sv-SOD1^{G93A} fold change = 1.5, *Q*-value: 0.000496; C57-SOD1^{G93A} fold change = 2.3 *Q*-value: 3.0×10^{-6}) and antigen peptide transporter 1 (*Tap1*; 129Sv-SOD1^{G93A} fold change = 1.5, *Q*-value: 0.00108; C57-SOD1^{G93A} fold change = 2.6; *Q*-value: 7.0×10^{-6}). Consistent with these findings, two immunoproteasome subunits normally involved in antigen processing and presentation through the MHCI complex (Muchamuel *et al.*, 2009; de Graaf *et al.*, 2011), large multifunctional peptidase 7 (*Lmp7*; fold change = 4.5, *Q*-value: 0.000118) and proteasome activator complex subunit 1 (*Psme1*; fold change = 2.4, *Q*-value: 4.1×10^{-8}), are upregulated specifically in C57-SOD1^{G93A} motor neurons (Fig. 5A–C and Supplementary Table 3). MHCI protein expression was analysed in the lumbar spinal cord of both transgenic mouse strains at the onset of the disease. Notably, although a clear signal of MHCI-immunoreactivity was detected in microglia and oligodendrocytes (Supplementary Fig. 6A–D), the motor neuron cell bodies were weakly immunolabelled (Fig. 5D–G). However, we were able to identify clear MHCI-immunoreactivity in cultured motor neurons from C57-SOD1^{G93A} mice that appear to overexpress MHCI compared to motor neurons from non-transgenic littermates (Supplementary Fig. 7). As it has been recently demonstrated that MHCI molecules produced in motor neuron somata are transported peripherally into motor axons (Medana *et al.*, 2001; Ishii and Mombaerts, 2008; Taylor *et al.*, 2009; Thams *et al.*, 2009), we analysed the sciatic nerves of both SOD1^{G93A} mouse strains and their respective non-transgenic littermates and demonstrated an increase of MHCI immunoreactivity in the sciatic nerve of C57-SOD1^{G93A} mice compared with non-transgenic controls and 129Sv-SOD1^{G93A} mice (Fig. 5H–O). In particular, MHCI-immunoreactivity was observed in a subpopulation of axons co-labelled with the axonal marker Smi31 in the sciatic nerve of C57-SOD1^{G93A} mice (Fig. 5P and Q). In order to verify that MHCI was confined to the motor axons in the sciatic nerves, we evaluated its expression in the sciatic nerve of B6.Cg-Tg(Hlxb9-GFP) mice with or without the SOD1^{G93A} transgene. These mice that express GFP under the direction of the mouse Hlxb9 promoter display selective production of GFP in dendrites, axons and somata of spinal motor neurons. These results confirm the specific localization and high expression of

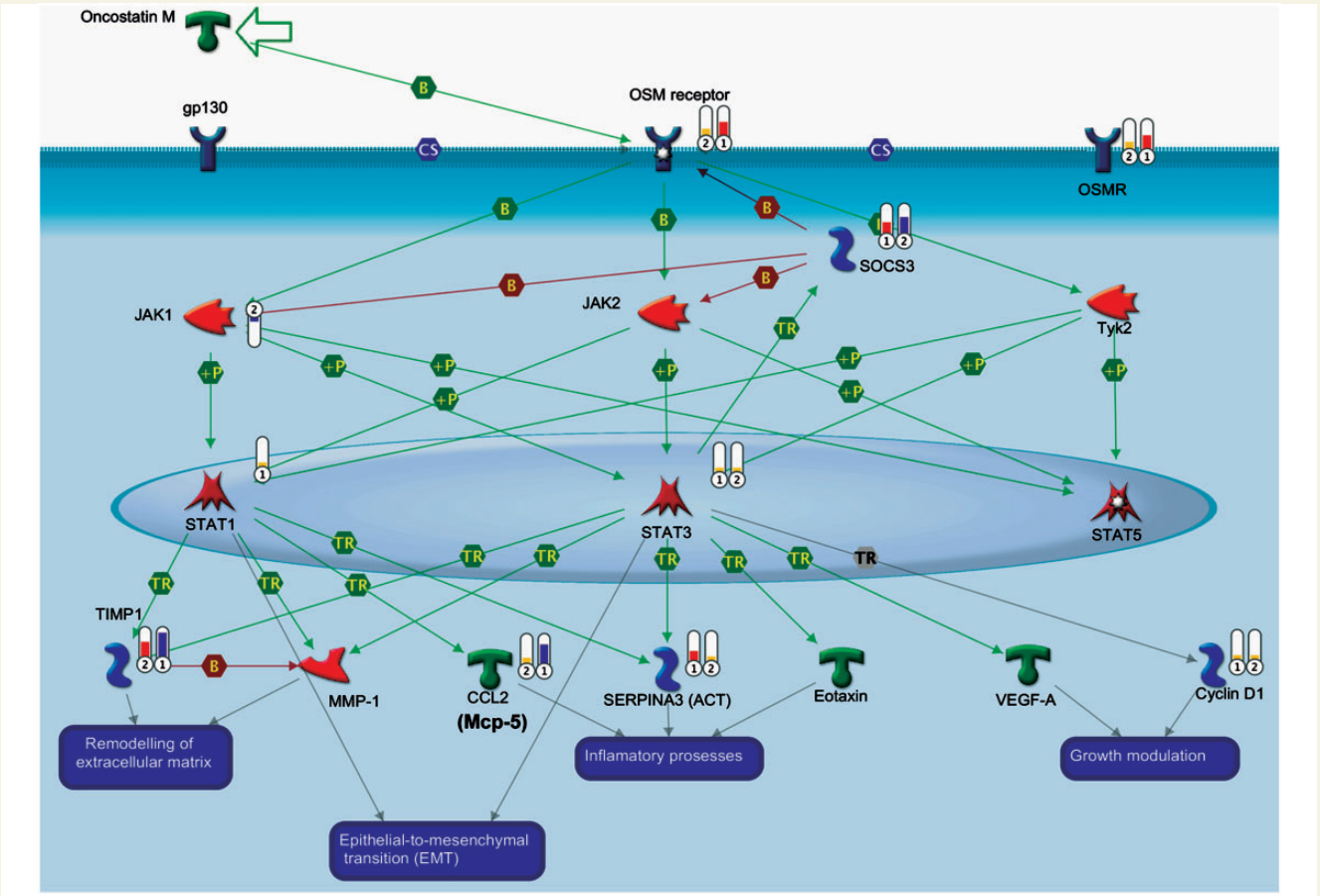

Figure 3 Oncostatin M signalling through the JAK-STAT pathway in C57-SOD1^{G93A} and 129SV-SOD1^{G93A} motor neurons at disease onset. Binding of oncostatin M to OSM receptor (OSMR) induces the Janus kinases (JAK)/signal transducer (JAK1, JAK2, Tyk2) and activation through phosphorylation, of transcription (STAT) signalling pathway (STAT1, STAT3, STAT5). Phosphorylated STATs then dimerize, translocate to the nucleus, bind to regulatory elements in the promoter of OSM-responsive genes and induce gene expression. Metacore^{TM} comparison analysis between the two transgenic mice at disease onset shows that: (i) OSM receptor is over-expressed in C57-SOD1^{G93A} motor neurons; (ii) SOCS3, which is an inhibitor of oncostatin M signals, is over-expressed in 129Sv-SOD1^{G93A} motor neurons; and (iii) the specific activation of STAT1 in C57-SOD1^{G93A} motor neurons may account for higher levels of expression of *SERPINA3* (*Serpina3n*), *CCL2* (*Mcp-5*) and *TIMP-1* (*Timp1*). Experimental data are visualized on the maps as thermometer-like symbols (1 = C57-SOD1^{G93A} mice; 2 = 129SV-SOD1^{G93A} mice). Upward thermometers indicate upregulated signals as indicated by the following fold-change ranges: 1–4 = orange; 4–8 = red; 8–13 = purple. Downward (blue) thermometers indicate downregulated expression levels of the genes. CS = complex subunit; B = binding; TR = transcription regulation; $^{+}$P = phosphorylation; green arrow indicates activation; red arrow indicates inhibition.

MHCI in sciatic GFP labelled-motor axons of GFP-SPM transgenic mice (Fig. 5R and S; Supplementary Fig. 8A–N). We next studied MHCI-immunoreactivity at the neuromuscular junctions of gastrocnemius muscles of transgenic and non-transgenic mice from both genetic backgrounds at the onset of the disease. The presynaptic motor terminals were stained with synaptophysin and the postsynaptic acetylcholine receptor clusters were visualized with alpha-bungarotoxin (α-btx). As for the sciatic nerve, greater levels of MHCI-immunoreactivity were observed at the neuromuscular junctions of C57-SOD1^{G93A} mice compared with the 129Sv-SOD1^{G93A} strain (Fig. 5T).

Angiogenin like-activity

Other clusters of transcripts specifically upregulated in C57-SOD1^{G93A} compared with 129Sv-SOD1^{G93A} motor neurons are those involved in extracellular matrix remodelling, endocytosis and lysosome activity (Fig. 2B). Amongst these categories, the most significant is the 'blood vessel development' functional category (EASE: 4.9). The 2D view map representing the internal relationships among the clustered terms and genes in this category is shown in Supplementary Fig. 9. Of the 22 genes belonging to this category, 21 are upregulated whereas one (fibroblast growth factor 18) is downregulated (Supplementary Table 6). Within the gene cluster it is possible to identify a subcategory of 12 transcripts involved in angiogenesis. Some of these genes (transforming growth factor receptor 1 and 2, *Ang*, angiopoietin 1) belong to the class of angioneurins, molecules that affect both neural and vascular cell functions (Zacchigna *et al.*, 2008).

In addition, the upregulation of the hypoxia inducible factor 1a is specifically related to the activation of vascular endothelial

Table 1 Transcripts involved in the onscostatin M pathway altered in C57-SOD1^{G93A} and 129Sv-SOD1^{G93A} motor neurons at disease onset

Probe set ID	Gene name	Gene symbol	Q-value C57	Fold change C57	Q-value 129Sv	Fold change 129Sv
1418674_at	Oncostatin M receptor	*Osmr*	1.14×10^{-16}	7.2	1.28×10^{-7}	3.2
1416576_at	Suppressor of cytokine signaling 3	*Socs3*	1.54×10^{-13}	5.7	3.9×10^{-11}	9.2
1433803_at	Janus kinase 1	*Jak1*	n.s.	n.c.	0.0051	−1.7
1459961_a_at	Signal transducer and activator of transcription 3	*Stat3*	0.0025	2.0	0.0015	1.9
1450034_at	Signal transducer and activator of transcription 1	*Stat1*	0.00015	1.6	n.s.	n.c.
1460227_at	Tissue inhibitor of metalloproteinase 1	*Timp1*	1.00×10^{-24}	13.0	4.44×10^{-12}	7.8
1419282_at	Chemokine (C-C motif) ligand 12	*CcL2 (Ccl12)*	6.38×10^{-8}	10.4	0.0035	2.5
1419100_at	Serine (or cysteine) peptidase inhibitor, clade A, member 3n	*Serpina3n*	8.17×10^{-12}	5.2	0.0066	1.8
1448698_at	Cyclin D1	*Ccnd1*	0.0017	1.6	0.005	1.5

(Q-value) Multiple hypothesis testing = Q-val[i] = mean (1-PPLR[1:i] where PPLR is the probability of positive log ratio (F.C.) Fold change = expressed as mean fold change ratio between four SOD1^{G93A} versus four non-transgenic mice; n.s. = not significant; n.c. = not classified.

growth factor and *Ang* through the binding to a hypoxia-response element in the promoter of their genes. In the light of recent findings demonstrating that ANG, a 14 kDa angiogenic ribonuclease, promotes motor neuron survival and has a beneficial effect on the disease course of SOD1^{G93A} mice (Kieran *et al.*, 2008; Sebastià *et al.*, 2009; Li and Hu, 2010), we further investigated the expression level of *Ang* in the two transgenic mice strains. *Ang* messenger RNA that was initially reduced in both transgenic mouse strains at the presymptomatic stage (data not shown), dramatically increased in the C57-SOD1^{G93A} but not in 129Sv-SOD1^{G93A} mice at the onset of the disease (Fig. 6A) and remained high during disease progression (data not shown). Immunohistochemical analysis performed at disease onset on the lumbar spinal cord of both transgenic mice and non-transgenic littermates, (Fig. 6B) clearly demonstrated that: (i) ANG immunoreactivity appears mostly confined to motor neurons in non-transgenic mice, but its intensity level is remarkably lower in 129Sv-SOD1^{G93A} versus C57-SOD1^{G93A} non-transgenic mice; and (ii) at disease onset ANG immunoreactivity appears highly expressed in structures surrounding the motor neurons in C57 mice whereas an overall reduction of immunoreactivity is observed in 129Sv-SOD1^{G93A} mice compared to their non-transgenic littermates. In contrast with messenger RNA expression, ANG immunoreactivity does not appear upregulated in the motor neurons of C57-SOD1^{G93A} mice in comparison with non-transgenic littermates whereas it was clearly decreased in the 129Sv-SOD1^{G93A} motor neurons compared with their non-transgenic littermates. These observations were confirmed by immunoblot analysis of the ventral horn from lumbar spinal cords performed at the same disease stage (Fig. 6C and D).

Downregulated mechanisms in 129Sv-SOD1^{G93A} motor neurons at disease onset

Functional annotation clustering performed on 1101 genes specifically altered in 129Sv-SOD1^{G93A} motor neurons at disease onset identified six gene clusters with an EASE >1.8, showing marked downregulation (Fig. 2C).

Mitochondrial transcripts and energy metabolism

The most striking cluster of genes encompassing transcripts that are strikingly downregulated in 129Sv-SOD1^{G93A} motor neurons at disease onset compared to C57-SOD1^{G93A} motor neurons is related to mitochondrial activity. The GO enrichment analysis performed through DAVID on transcripts differentially expressed between 129Sv-SOD1^{G93A} and non-transgenic littermates identified as the most significant the mitochondrion gene cluster (GO: 0005739; EASE: 29.3). Of the 191 genes within this category, 187 are downregulated (Supplementary Table 7).

Notably, dihydrolipoamide S-acetyltransferase (E2; fold change = −1.7, *Q*-value: 0.000016) and dihydrolipoamide dehydrogenase (E3; fold change = −1.6, *Q*-value: 0.0062) pyruvate dehydrogenase subunits are downregulated. The predicted impairment of pyruvate metabolism is inline with a widespread dysregulation of key enzyme subunits involved in the normal function of the citric acid cycle and the electronic transport chain (oxidative phosphorylation KEGG pathway; *P*-value: 2.0×10^{-21}). Among the electronic transport chain complexes, NADH dehydrogenases (complex I) and ATP synthase are the most compromised with altered expression of 23 and seven subunits, respectively (Supplementary Fig. 10 and Supplementary Table 8). The predicted impairment in ATP production is likely to be further exacerbated by the downregulation of creatine kinase^{mt}, an enzyme that produces phosphocreatine from mitochondrially-generated ATP (Wallimann *et al.*, 1992). On the basis of these alterations in gene expression, we measured complex I activity and the ATP concentration (nmol/mg) directly in tissue, confirming a marked decrease in energy production in the ventral portion of the lumbar spinal cord of 129Sv-SOD1^{G93A} motor neurons compared with C57-SOD1^{G93A} (Supplementary Fig. 11A–C). The mitochondrial dysregulation is further confirmed by the downregulation of 22 mitochondrial ribosomal subunits (Supplementary Table 8) and the upregulation of the uncoupling protein 2, a key marker of

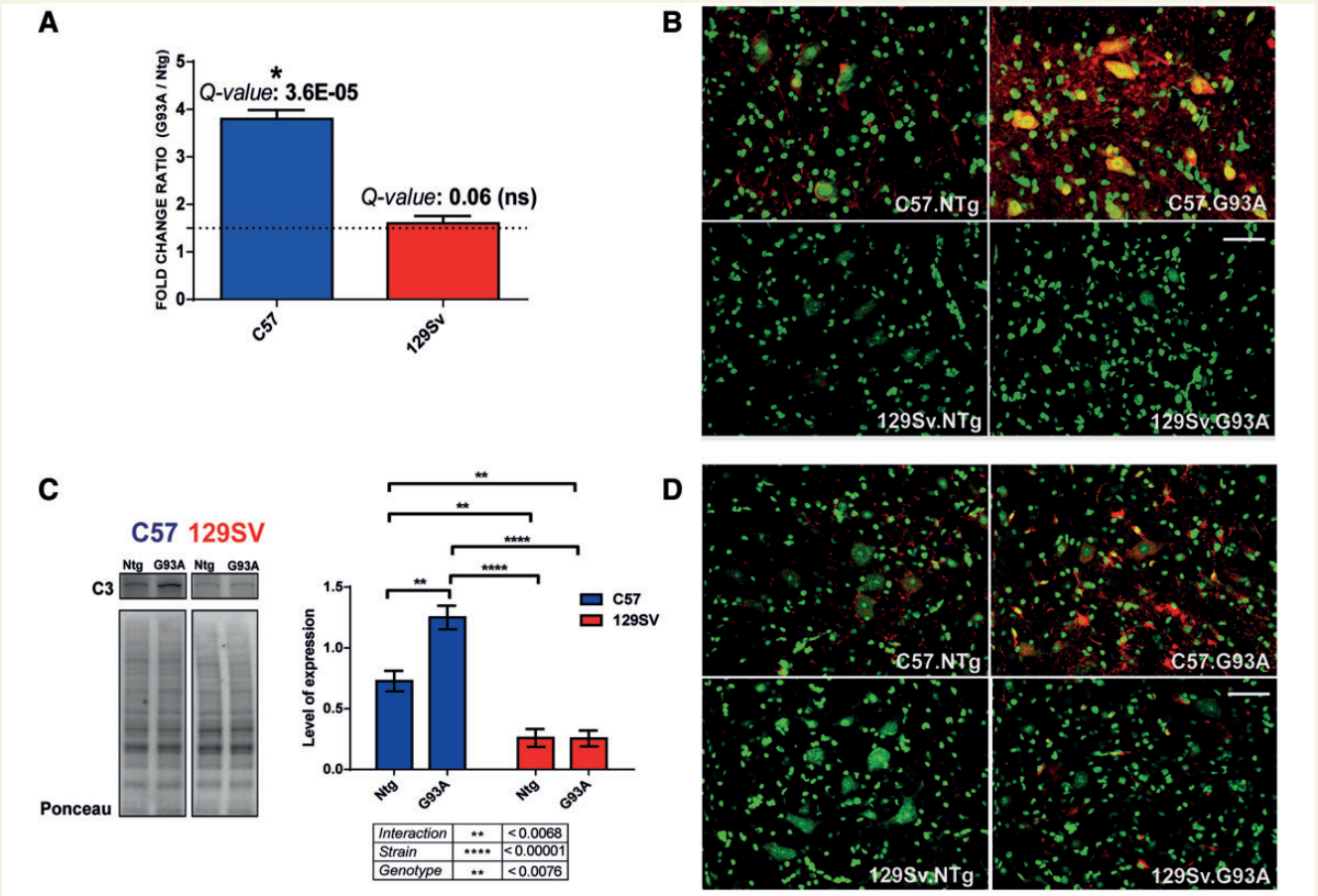

Figure 4 Analysis of C3 and C3 activated by-products at disease onset. (**A**) *C3* messenger RNA levels are specifically increased in the C57-SOD1^{G93A} motor neurons (fold change = 3.8). Messenger RNA levels are reported as mean fold-change ratio [± standard error (SE)] between SOD1^{G93A} (n = 4) and non-transgenic (n = 4) mice in C57-SOD1^{G93A} and 129Sv-SOD1^{G93A} motor neurons (dotted line defines the fold-change of 1.5). Q-values were generated from PPLR using the following formula: *Q-val*[i] = mean (1 − PPLR[1:i]); *Q-value ⩽ 0.01; ns = not significant. (**B**) Immunohistochemical comparison, performed at disease onset on lumbar spinal cord of C57-SOD1^{G93A}, 129Sv-SOD1^{G93A} and non-transgenic littermates (C3 = red; neurotrace = green) showing: (i) the expression of C3 by motor neurons; (ii) higher basal levels of C3 in C57-Ntg compared with 129sv-Ntg mice; and (iii) the induction of C3 within C57-SOD1^{G93A} motor neurons. Scale bar = 50 μm. (**C**) C3 western blot analysis on longitudinally dissected lumbar ventral spinal cord protein extracts from C57-SOD1^{G93A}, 129Sv-SOD1^{G93A} and non-transgenic littermates at disease onset. Immunoreactivity was normalized to the actual amount of proteins loaded on the membrane as detected after Red Ponceau (Fluka). Densitometric analysis of C3 levels further confirms the immunohistochemical findings. The graph represent the mean ± SE of four mice per group. Two-way statistical analysis shows significant interaction (F = 10.63) due to genotype (non-transgenic: G93A − F = 81.65) and strain (129Sv: C57 − F = 10.64) (Tukey's *post hoc* $^{**}P < 0.01$; $^{****}P < 0.0001$). (**D**) Immunohistochemical comparison performed at disease onset on lumbar spinal cord of C57-SOD1^{G93A}, 129Sv-SOD1^{G93A} and non-transgenic littermates, showing an induction of C3 activated fragments (C3a/C3b/iC3b/C3c) within C57-SOD1^{G93A} motor neurons at disease onset. Scale bar = 50 μm.

mitochondrial stress (fold change = 3.0, Q-value: 0.000239) (Mills *et al.*, 2002; Serviddio *et al.*, 2008).

Ubiquitin proteasome system

The 'protein catabolic process' represents the second significant gene cluster (GO: 0030163; EASE: 5.2) specifically downregulated in motor neurons from 129Sv mice at disease onset (Fig. 2C).

Twenty genes coding for E2 ubiquitin conjugating enzymes, E3 ubiquitin-protein ligase enzymes and adaptor proteins involved in the ubiquitin proteasome system show decreased expression in 129Sv-SOD1^{G93A} motor neurons as illustrated in the KEGG pathway 'ubiquitin mediate proteolysis' (P-value: 4.5×10^{-2}) (Supplementary Fig. 12 and Supplementary Table 9). Among them, ubiquitin-conjugating enzyme E2A, ubiquitin-conjugating enzyme E2N and PRP19/PSO4 pre-messenger RNA processing factor 19 homologue have a supplementary role in DNA repair (Ashley *et al.*, 2002; Carninci *et al.*, 2005; Karras and Jentsch, 2010). In addition, proteasome complex-associated transcripts including six subunits belonging to the 19S regulatory particle and eight subunits belonging to the 20S 'core' particle (proteasome KEGG pathway; P-value: 1.42×10^{-9}), show decreased messenger RNA levels in the rapid progressor mouse strain (Supplementary Fig. 13 and Supplementary Table 10).

Notably, the deubiquitinases proteasome-associated enzyme, Ubiquitin C-terminal hydrolase 37 (*Uch37*) is downregulated in

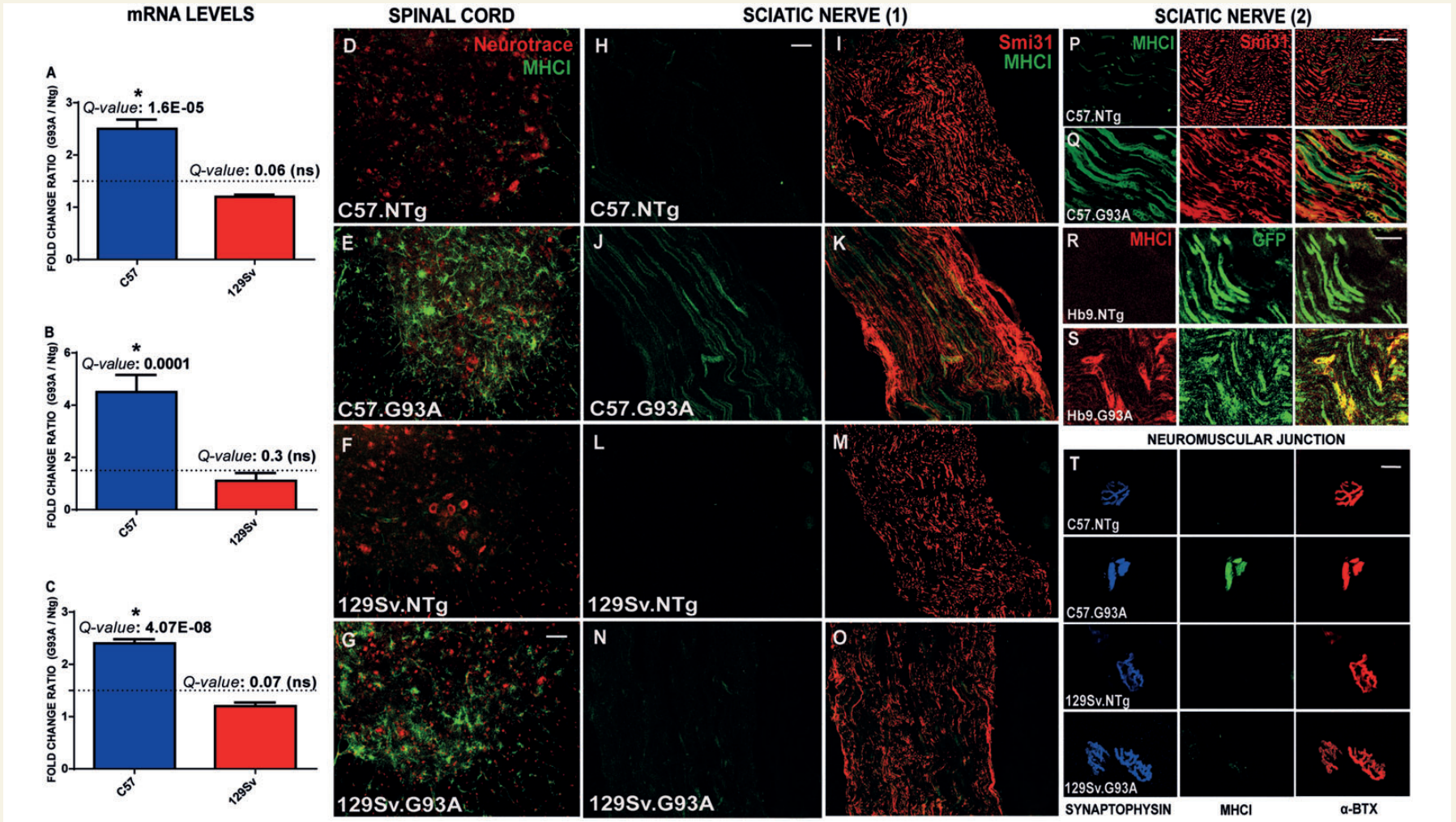

Figure 5 Analysis of MHCI expression at disease onset. (**A–C**) *Mhcl* (**A**), *Lmp7* (**B**) and *Psme1* (**C**) messenger RNA levels are specifically increased within C57-SOD1^{G93A} motor neurons (*Mhcl*, fold change = 2.5; *Lmp7*, fold change = 4.5; *Psme1*, fold change = 2.7). Messenger RNA levels are expressed as mean fold-change ratio (±SE) between SOD1^{G93A} ($n = 4$) and non-transgenic ($n = 4$) mice, in C57-SOD1^{G93A} and 129Sv-SOD1^{G93A} mice (dotted lines defines the fold-change of 1.5). *Q*-values were generated from PPLR using the following formula: *Q-val*[i] = mean (1 − PPLR[1:i]); **Q*-value ⩽ 0.01; ns = not significant. (**D–G**) Confocal micrographs from the ventral lumbar spinal cord of C57-SOD1^{G93A}, 129Sv SOD1^{G93A} and non-transgenic littermates at disease onset illustrating: (i) the activation of MHCI (green) in both transgenic mice strain at disease onset; and (ii) low MHCI immunoreactivity within motor neuron perikarya. Neurotrace = red. Scale bar = 50 μm. (**H–O**) Confocal micrographs from the sciatic nerve of C57-SOD1^{G93A}, 129Sv-SOD1^{G93A} and non-transgenic littermate mice showing higher MHCI levels (green) in the sciatic nerve of C57-SOD1^{G93A} mice at disease onset. Smi31 (red) putative motor axons. Scale bar = 50 μm. (**P** and **Q**) Sciatic nerve magnification from both C57-NTg and C57-SOD1^{G93A} mice at disease onset illustrating MCHI (green) activation and co-localization with Smi31 (red) in axons from the diseased mice. Scale bar = 50 μm. (**R** and **S**) Sciatic nerve magnification from B6.Cg-Tg(Hlxb9-GFP)-SOD1^{G93A} mice and non-transgenic littermates at disease onset showing the co-localization of GFP (green, exclusively expressed by motor axons), with MHCI (red) in the diseased mice. Scale bar = 50 μm. (**T**) Confocal micrographs of neuromuscular junctions from C57-SOD1^{G93A}, 129Sv-SOD1^{G93A} and non-transgenic littermates at disease onset showing the co-localization of synaptophysin (blue, presynaptic marker), MHCI (green) and α-bungarotoxin (α-btx, red, postsynaptic marker) in the gastrocnemius muscle specifically in the C57-SOD1^{G93A} mice.

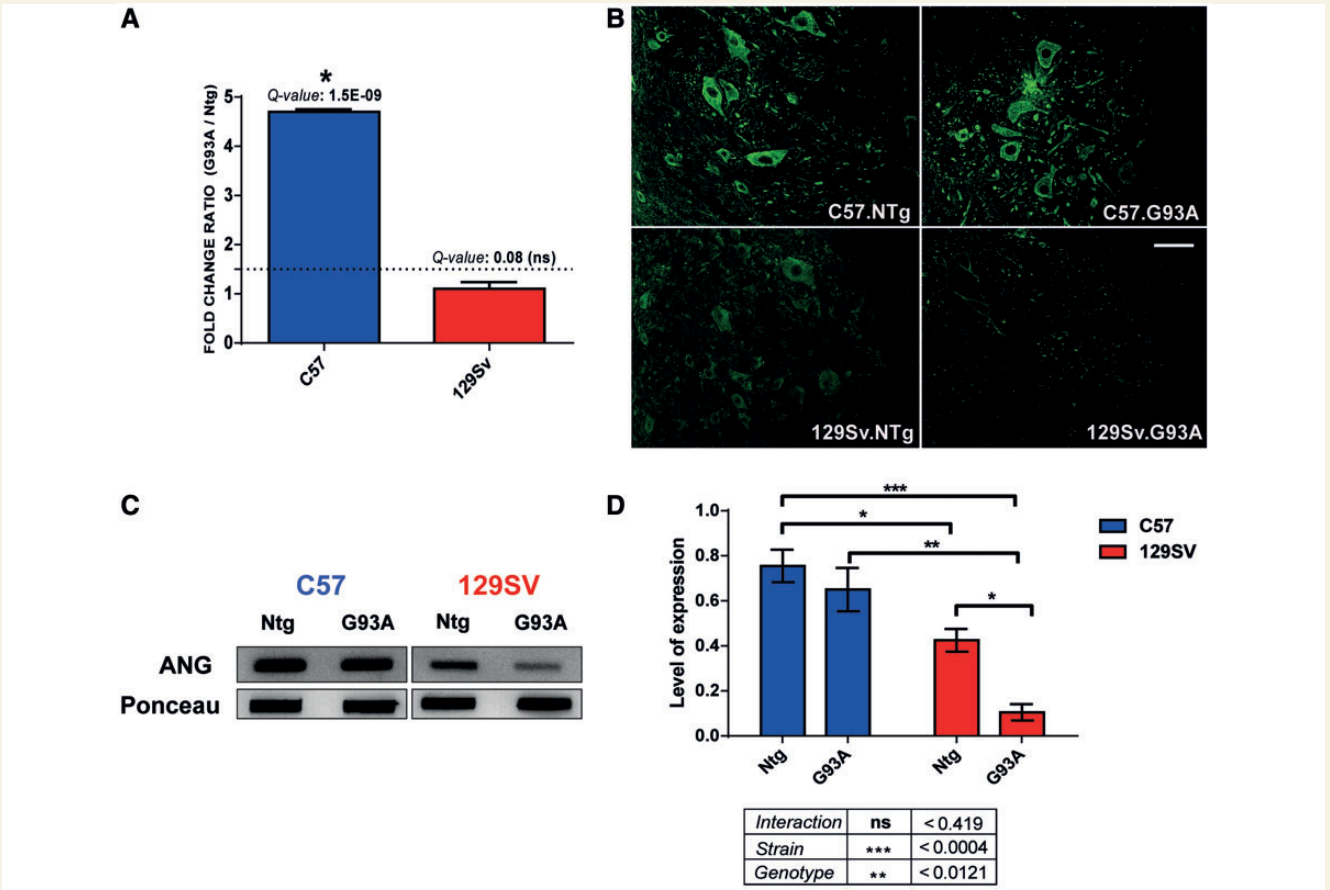

Figure 6 Analysis of ANG expression at disease onset. (**A**) *Ang* messenger RNA levels are specifically increased in the C57-SOD1^{G93A} motor neurons (fold change = 4.7). Messenger RNA levels are reported as mean fold change ratio (±SE) between SOD1^{G93A} ($n = 4$) and non-transgenic ($n = 4$) mice, in 129Sv-SOD1^{G93A} and C57-SOD1^{G93A} motor neurons (dotted line defines the fold-change of 1.5). *Q*-values were generated from PPLR using the following formula: *Q-val*[i] = mean (1 − PPLR[1:i]); *Q-value ⩽ 0.01; ns = not significant. (**B**) Immunohistochemical comparison, performed at disease onset on lumbar spinal cord of C57-SOD1^{G93A}, 129Sv-SOD1^{G93A}, and non-transgenic littermates, showing: (i) the predominant expression of ANG by motor neurons; (ii) lower ANG basal levels in 129Sv-Ntg versus C57-Ntg mice; and (iii) reduction in ANG expression in 129Sv-SOD1^{G93A} motor neurons at disease onset. Scale bar = 50 μm. (**C**) ANG slot-blot analysis on longitudinally dissected lumbar ventral spinal cord protein extracts from C57-SOD1^{G93A}, 129Sv-SOD1^{G93A} and non-transgenic littermates at disease onset. Immunoreactivity was normalized to the actual amount of proteins loaded on the membrane, as detected after Red Ponceau (Fluka). (**D**) Densitometric analysis of ANG levels confirms the immunohistochemical findings. Data are reported as mean ± SE of four mice per group. Two-way statistical analysis shows the effect of strain (129Sv; C57 − F = 41.59) and the genotype (non-transgenic; G93A − F = 9.81) on the overall variability. Tukey's *post hoc* *$P < 0.05$; **$P < 0.01$; ***$P < 0.001$.

129Sv motor neurons at disease onset (Fig. 7A). UCH37 is responsible for the ubiquitin isopeptidase activity in the PA700 (19S) proteasome regulatory complex which disassembles Lys 48-linked polyubiquitin specifically from the distal end of the chain promoting proteasomal protein degradation (Lee *et al.*, 2011). Immunohistochemistry and immunoblot analysis of the ventral portion of lumbar spinal cord confirmed that *Uch37* messenger RNA dysregulation correlates with downregulation of UCH37 protein expression in 129Sv-SOD1^{G93A} motor neurons at disease onset (Fig. 7B–D).

Vesicle trafficking and protein transport

According to the DAVID analysis, the protein transport category represents the third most significantly altered gene functional cluster (GO: 0015031; EASE: 3.22) in 129Sv-SOD1^{G93A} motor neurons at disease onset. There is widespread dysregulation of multiple soluble *N*-ethylmaleimide-sensitive factor attachment proteins (SNAREs) (YKT6 homologue, *N*-ethylmaleimide sensitive fusion protein attachment protein alpha, *N*-ethylmaleimide sensitive fusion protein attachment protein gamma, vesicle-associated membrane protein 7) as well as small GTPase Rab proteins (Ras-related protein Rab-2a, Ras-related protein Rab2b, Ras-related protein Rab11a) (Zerial and McBride, 2001; Jahn and Scheller, 2006; Sann *et al.*, 2009; Jena *et al.*, 2011). The activity of these molecules is principally implicated in the transport of vesicles between endoplasmic reticulum–Golgi, Golgi–endosome, early/late endosome-lysosome and Golgi-plasma membrane (Supplementary Fig. 14 and Supplementary Table 11). Notably, the vesicle-associated membrane protein-associated protein B and C, mutations in which are associated with human ALS, is downregulated (Chen

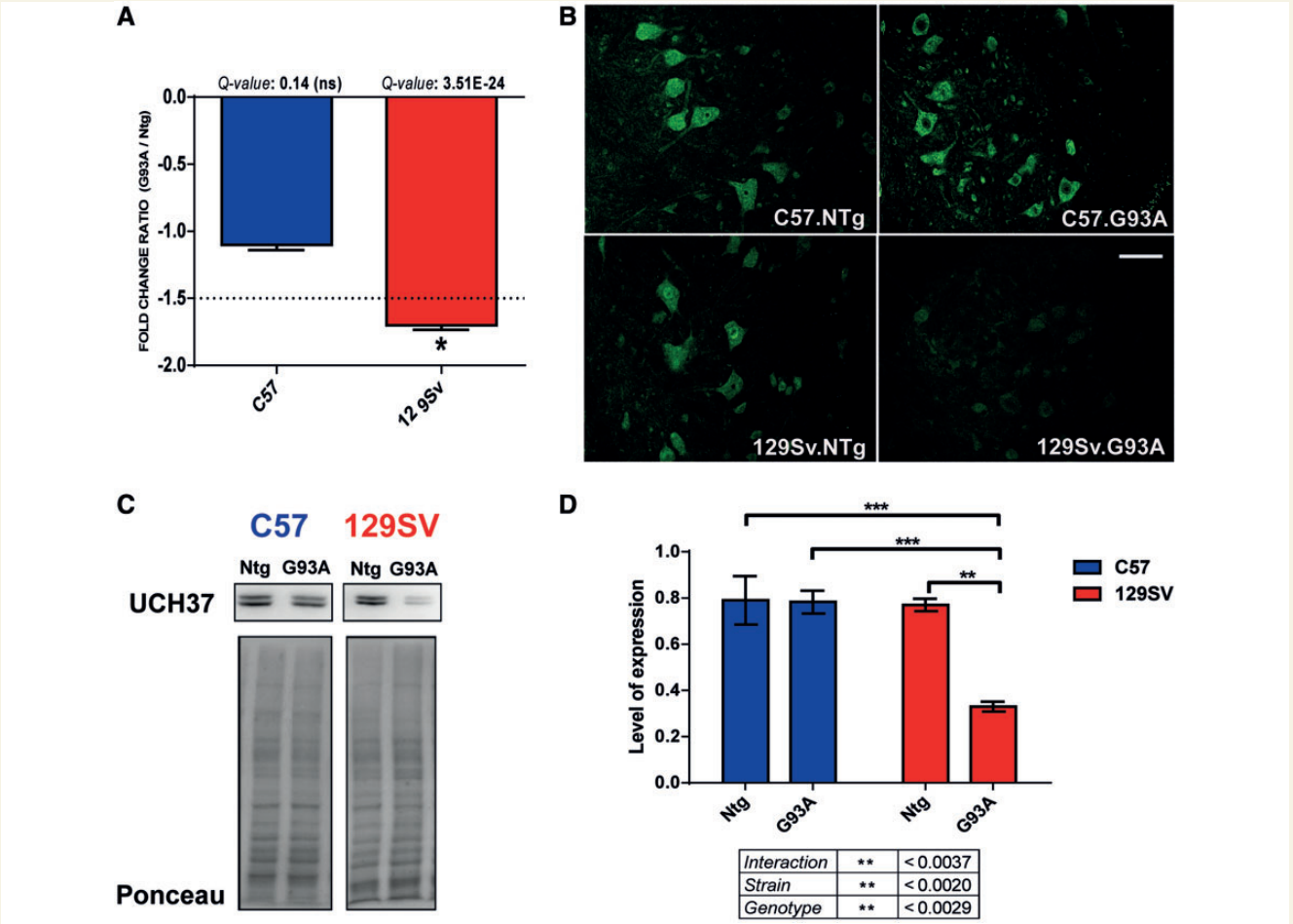

Figure 7 Analysis of UCH37 expression at disease onset. (**A**) *Uch37* messenger RNA levels are specifically reduced in the 129Sv-SOD1^{G93A} motor neurons. Messenger RNA levels are reported as mean fold-change ratio (±SE) between SOD1^{G93A} ($n = 4$) and non-transgenic ($n = 4$) mice in 129Sv-SOD1^{G93A} and C57-SOD1^{G93A} motor neurons (dotted line defines the fold-change of −1.5). Q-values were generated from PPLR using the following formula: *Q-val*[i] = mean (1 − PPLR[1:i]); *Q-value ⩽ 0.01; ns = not significant. (**B**) Immunohistochemical comparison performed at disease onset on lumbar spinal cord of C57-SOD1^{G93A}, 129Sv-SOD1^{G93A} and non-transgenic littermates showing: (i) the expression of UCH37 by motor neurons; and (ii) lower levels of UCH37 in motor neurons from 129Sv-SOD1^{G93A} mice. Scale bar = 50 μm. (**C**) UCH37 western blot analysis on longitudinally dissected lumbar ventral spinal cord protein extracts from C57-SOD1^{G93A}, 129Sv-SOD1^{G93A} and non-transgenic littermates at disease onset. Immunoreactivity was normalized to the actual amount of protein loaded on the membrane as detected after Red Ponceau (Fluka). (**D**) Densitometric analysis of UCH37 levels confirms the immunohistochemical findings. Data are reported as mean ± SE of four mice per group. Two-way statistical analysis shows significant interaction (F int. = 12.92) due to strain (129Sv; C57 − F = 15.43) and genotype (non-transgenic; G93A − F = 0.70) Tukey's *post hoc* $^{**}P < 0.01$; $^{***}P < 0.001$.

et al., 2010). The level of this impairment extends to involve molecules important in organelle function such as the component of oligomeric Golgi complex 1 and component of oligomeric Golgi complex 8 that influence Golgi morphology and localization (Carninci *et al.*, 2005; Chatterton *et al.*, 1999) or vacuolar protein sorting 24 and chromatin modifying protein 2B that regulate endosome maturation. (Skibinski *et al.*, 2005; Nickerson *et al.*, 2006). Different components of the nuclear pore complex (importin 4, karyopherin alpha 1, transportin 2) are downregulated with all the implications that this may confer on the bidirectional communication between the nuclear and cytoplasmic compartments. Similarly, the activity of the respiratory chain is likely to be indirectly compromised through the dysregulation of different translocases of the inner mitochondrial (*Tim*) membrane (*Timm10*, *Timm17*, *Timm23*) and one translocase of the outer mitochondrial (*Tom*) membrane (*Tomm7*) involved in the import and insertion of multi-pass transmembrane proteins at the mitochondrial level.

Organization of neuronal projections

Neuron projection and microtubule categories represent, respectively, the fourth (GO: 0043005; EASE: 2.1) and the fifth (GO: 0005874; EASE: 1.8) gene clusters, in order of significance, related to 1101 transcripts specifically altered in 129Sv-SOD1^{G93A} motor neurons at disease onset (Fig. 2C). Although represented as two independent categories, they show inter-dependency as

microtubule stability has a fundamental role in the viability of motor axons.

Motor axon morphology and functionality are likely to be negatively influenced by the dysregulation of two tubulin subunits (tubulin alpha 4A; tubulin beta 2C) and several transcripts controlling microtubule polarization (microtubule-associated protein 1 A; microtubule-associated protein 9; tubulin polyglutamylase complex subunit 1) (Denarier *et al.*, 1998; Nakayama *et al.*, 2001; Regnard *et al.*, 2003) and axonal/synapse stability and regeneration (stathmin-like 2; utrophin; cysteine-rich PDZ-binding protein) (Bhosle *et al.*, 2006; Tararuk *et al.*, 2006; Saro *et al.*, 2007) (Supplementary Table 12). Interestingly, different transcripts involved in anterograde and retrograde axonal transport are specifically downregulated in 129Sv-SOD1^{G93A} motor neurons. We found the decreased expression of two non-catalytic (dynein light chain Tctex-type 3; dynein, cytoplasmic 1 light intermediate chain 2) components involved in linking dynein 1 to cargos and to adapter proteins that regulate its function (Lo *et al.*, 2007; Palmer *et al.*, 2009). In addition, six kinesin heavy chain isoforms and one kinesin light chain isoform with heterogeneous activities within motor axons (microtubule turnover; mitochondrial and lysosome translocation; neurofilament transport) (Adalbert and Coleman, 2012; Millecamps and Julien, 2013) are downregulated Supplementary Table 12). We analysed the protein expression levels of kinesin heavy chain isoform 5a (*Kif5a*), 5b (*Kif5b*) and 5c (*Kif5c*) the activity of which in adult motor neurons was reported to be essential in maintaining normal cell homeostasis (Kanai *et al*., 2000; Xia *et al*., 2003; Cho *et al*., 2007). Immunoblot and immunohistochemical comparison, performed using an antibody specifically directed against the three heavy chain isoforms, further validate a marked downregulation of KIF5A, KIF5B and KIF5C in 129Sv-SOD1^{G93A} motor neurons at disease onset (Fig. 8A–C).

Overconnected transcription factors

The interactome topology performed on both whole transgenic mice data sets at the onset of the disease show a clustering coefficient (density of connections) of 0.06 for C57-SOD1^{G93A} versus 0.04 for 129Sv-SOD1^{G93A} highlighting a lower molecular complexity of the 129Sv-SOD1^{G93A} gene network (Supplementary Table 13). The 'interactome tool' in Metacore^{TM} allows estimation of the interconnectedness of elements of the experimental data set (density of interactions), finding statistically significant interactions in the set and enrichment of the data set with protein classes. In particular, this tool allows the identification of statistically significant data objects that interact with and regulate other proteins, representing potential disease and process biomarkers. We used this application to identify over-connected transcription factors within the gene profiles of the two transgenic mouse strains. Over-connected transcription factors have a number of interactions more than (or equal to) the mean (mathematical expectation) and a Z-score $\geqslant 0$. A false discovery rate (FDR) $\leqslant 0.05$ was selected as threshold in order to reject false positives and data objects of doubtful significance.

The analysis showed a greater number of over-connected transcription factors in the C57-SOD1^{G93A} than in the 129Sv-SOD1^{G93A} data set (Table 2). Notably, the number of interactions of common transcription factors is greater within the C57-SOD1^{G93A} network: *STAT3* and tripartite motif-containing protein 14 (*PU.1*) significantly interacts with 88 and 95 active network objects, respectively versus 76 and 79 in the 129Sv-SOD1^{G93A} network. Among the over-connected transcription factors, we analysed the protein expression of activating transcription factor 3 (*Atf3*) and *Nrf2* as representative markers of neuronal regenerative/injury response. In particular, ATF3 levels of expression are directly proportional to the degree of ubiquitin protein aggregation inside motor neurons (Tsujino *et al.*, 2000; Vlug *et al.*, 2005). According to our microarray data, *Atf3* messenger RNA levels are consistently higher in 129Sv-SOD1^{G93A} versus C57-SOD1^{G93A} motor neurons at the presymptomatic stage [C57-SOD1^{G93A}, fold change = 1.1; Q-value: 0.3 (not significant); 129Sv-SOD1^{G93A}, fold change = 11.7, Q-value: 6.67×10^{-16}] and disease onset (C57-SOD1^{G93A}, fold change = 9.8; Q-value: 7.84×10^{-11}; 129Sv-SOD1^{G93A}, fold change = 29.8; Q-value: 1.00×10^{-24}) (Fig. 9 A). Immunohistochemistry and immunoblot analysis (Fig. 9B–D) reveal: (i) a significant difference in the basal levels of ATF3, that is more expressed in C57 than 129Sv motor neurons; (ii) a significant upregulation of ATF3 in 129Sv-SOD1^{G93A} motor neurons versus non-transgenic littermates that accounts for the huge difference in messenger RNA levels (G93A/non-transgenic ratio) between the two mice strains at the onset of the disease; and (iii) no significant variation in ATF-3 protein levels in C57-SOD1^{G93A} mice versus non-transgenic littermates.

NRF2 is a transcription factor that interacts with the antioxidant response element enhancer sequence, to promote expression of proteins involved in the response to oxidative stress (Barber and Shaw, 2010). The expression of *Nrf2* messenger RNA increased in the motor neurons of C57-SOD1^{G93A} from disease onset (Fig. 10A), whereas in 129Sv-SOD1^{G93A} motor neurons we observed an increase in *Nrf2* levels only at the end stage of the disease (data not shown). In contrast with the messenger RNA levels, immunohistochemical analysis performed on lumbar spinal cord of both transgenic mice and relevant non-transgenic littermates at the onset of the disease identified no upregulation of NRF2 protein in C57-SOD1^{G93A}, whereas a reduction occurred in 129Sv-SOD1^{G93A} motor neurons (Fig. 10B). Immunoblot analysis of longitudinal dissected ventral horns further validate the immunohistochemical observations at the onset of the disease showing reduced NRF2 expression in 129Sv-SOD1^{G93A} motor neurons (Fig. 10C and D).

Discussion

This study provides the first detailed longitudinal comparison of the gene expression profiles of laser captured motor neurons from two SOD1^{G93A} mouse strains with different disease phenotypes. We demonstrate that a dramatic downregulation of gene expression characterizes motor neurons from the rapid progressor 129Sv-SOD1^{G93A} mice compared with the slow progressor C57-SOD1^{G93A} mice at the onset of the disease. The impairment predicted by gene expression changes of specific pathways involved in mitochondrial function, misfolded protein degradation, protein transport and neuron projections is particularly relevant in the

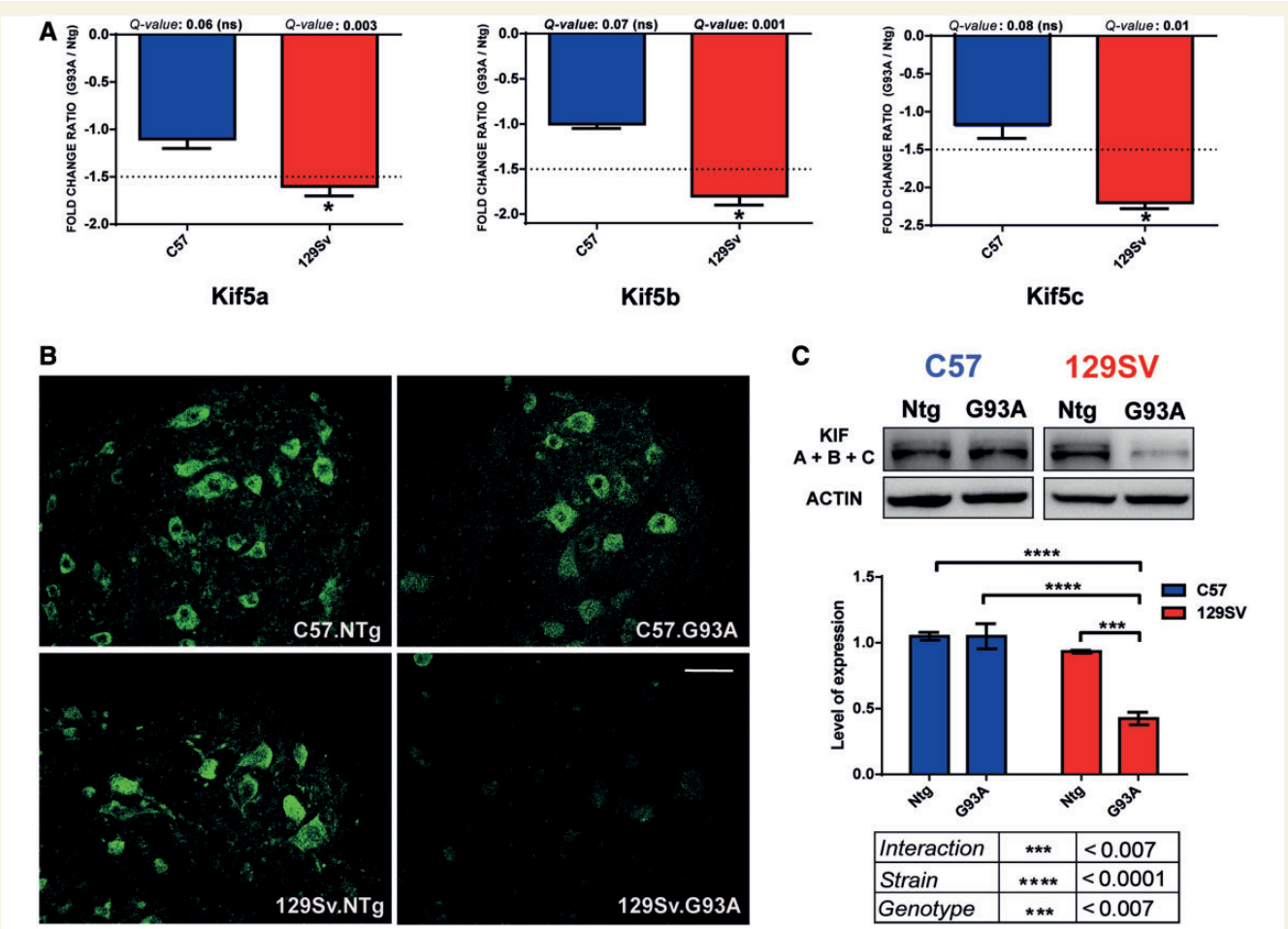

Figure 8 Analysis of KIF5A; KIF5B; KIF5C expression at disease onset. (**A**) *Kif5a*; *Kif5b* and *Kif5c* messenger RNA levels are specifically reduced in the 129Sv-SOD1^{G93A} motor neurons (*Kif5a*, fold-change = −1.6; *Kif5b*, fold-change = −1.8; *Kif5c*, fold-change = −2.2). Messenger RNA levels are reported as mean fold-change ratio (±SE) between SOD1^{G93A} ($n = 4$) and non-transgenic ($n = 4$) mice in 129Sv-SOD1^{G93A} and C57-SOD1^{G93A} motor neurons (dotted line defines the fold-change of −1.5). *Q*-values were generated from PPLR using the following formula: *Q-val*[i] = mean (1 − PPLR[1:i]); **Q*-value ⩽ 0.01; ns = not significant. (**B**) Immunohistochemical comparison performed at disease onset on lumbar spinal cord of C57-SOD1^{G93A}, 129Sv-SOD1^{G93A} and non-transgenic littermates showing: (i) the expression of KIF5A + B + C by motor neurons; and (ii) lower levels of the three proteins in motor neurons from 129Sv-SOD1^{G93A} mice. Scale bar = 50 μm. (**C** and **D**) KIF A + B + C western blot analysis on longitudinally dissected lumbar ventral spinal cord protein extracts from C57-SOD1^{G93A}, 129Sv-SOD1^{G93A}, and non-transgenic littermates at disease onset. Immunoreactivity was normalized to β-actin. Densitometric analysis of KIF A + B + C levels confirm the immunohistochemical findings. Data are reported as the mean ± SE of four mice per group. Two-way statistical analysis shows significant interaction (F int. = 20.75) due to strain (129Sv; C57 − F = 44.41) and genotype (non-transgenic; G93A − F = 20.75). Tukey's *post hoc* ***$P < 0.001$; ****$P < 0.0001$.

129Sv-SOD1^{G93A} motor neurons. In contrast, C57-SOD1^{G93A} motor neurons show activation of specific biological processes that may underpin a more consistent response to stress. In particular, GO pathway analysis of the transcriptional profile of C57-SOD1^{G93A} motor neurons at disease onset revealed a strong upregulation of genes related to immune system processes, as well as neuroprotective signalling pathways controlled by ANG and NRF2.

Neuroprotective immune system signalling pathways

A careful analysis of differential expression of immune transcripts common to both transgenic mice reveals that C57-SOD1^{G93A} motor neurons are more reactive to immune system stimuli than 129Sv-SOD1^{G93A} motor neurons. Pro-inflammatory (tumour necrosis factor receptor superfamily member 1a and 1b; interleukin 6 receptor alpha) and anti-inflammatory (interleukin 2 receptor gamma chain, colony stimulating factor 2 receptor beta, transforming growth factor, beta receptor I and II and interleukin 10 receptor beta) cytokine receptors show higher messenger RNA levels in C57-SOD1^{G93A} than in 129Sv-SOD1^{G93A} motor neurons. Amongst these, *Osmr* is expressed at a much higher level in C57-SOD1^{G93A} motor neurons. Oncostatin M is a pleiotropic cytokine of the interleukin 6 family, whose *in vivo* properties and physiological function remain controversial and poorly defined (Chen and Benveniste, 2004). However, recent data show that oncostatin M potently suppressed inflammation and tissue destruction in murine

Table 2 Interaction by protein function: over-connected transcription factors in C57-SOD1^{G93A} and 129Sv-SOD1^{G93A} motor neurons at disease onset

IDs in active data set[a]	F.C.[b]	Q-value[c]	Object name[d]	Actual[e]	n[f]	R[g]	n[h]	Expected[i]	Ratio[j]	Z-score[k]	P-value[l]
C57-SOD1^{G93A}											
1418747_at	1.6	0.002782	PU.1	95	1216	445	21012	25.8	3.7	14.2	2.644×10^{-29}
1450034_at	1.6	0.000154	STAT1	101	1216	621	21012	35.9	2.8	11.3	1.83×10^{-21}
1418901_at	1.5	0.000423	C/EBPbeta	103	1216	781	21012	45.2	2.3	9.0	2.665×10^{-15}
1448452_at	6.3	1.005×10^{-12}	IRF8	35	1216	133	21012	7.7	4.5	10.2	1.873×10^{-14}
1418982_at	1.9	0.000100	C/EBPalpha	79	1216	545	21012	31.5	2.5	8.8	3.648×10^{-14}
1459961_a_at	2.0	0.002581	STAT3	88	1216	660	21012	38.2	2.3	8.4	1.693×10^{-13}
1417065_at	2.1	0.000001	EGR1	92	1216	737	21012	42.7	2.2	7.9	2.191×10^{-12}
1437247_at	1.6	0.001732	Fra-2	25	1216	85	21012	4.9	5.1	9.3	6.901×10^{-12}
1427418_a_at	2.1	0.000390	HIF1A	73	1216	571	21012	33.0	2.2	7.3	1.507×10^{-10}
1449363_at	9.8	7.841×10^{-11}	ATF-3	29	1216	143	21012	8.3	3.5	7.4	2.68×10^{-09}
1423100_at	2.0	0.000011	c-Fos	61	1216	511	21012	29.6	2.1	6.0	6.413×10^{-08}
1426031_a_at	−1.6	0.010581	NF-AT1(NFATC2)	23	1216	138	21012	8.0	2.9	5.5	4.239×10^{-06}
1418932_at	1.6	0.001782	E4BP4 (NFIL3)	18	1216	101	21012	5.8	3.1	5.2	1.791×10^{-05}
1423233_at	6.3	1.222×10^{-14}	C/EBP	42	1216	366	21012	21.2	2.0	4.7	1.863×10^{-05}
1422864_at	2.5	3.384×10^{-07}	AML1 (RUNX1)	44	1216	399	21012	23.1	1.9	4.5	3.174×10^{-05}
1417394_at	1.6	0.001649	KLF4	30	1216	241	21012	13.9	2.2	4.5	6.449×10^{-05}
1422864_at	2.5	3.384×10^{-07}	AML1/ETO	15	1216	84	21012	4.9	3.1	4.7	8.565×10^{-05}
1417487_at	2.0	0.000782	Fra-1	14	1216	80	21012	4.6	3.0	4.5	0.0001825
1417516_at	2.2	4.95×10^{-09}	C/EBP zeta	22	1216	169	21012	9.8	2.2	4.0	0.0003104
1451538_at	1.7	0.000033	SOX9	24	1216	219	21012	12.7	1.9	3.3	0.002025
1427682_a_at	4.2	8.724×10^{-13}	EGR2 (Krox20)	16	1216	130	21012	7.5	2.1	3.2	0.003458
1447448_s_at	1.5	0.001126	KLF6	12	1216	85	21012	4.9	2.4	3.3	0.0035085
1421322_a_at	1.7	0.000283	IRF9	9	1216	55	21012	3.2	2.8	3.4	0.0040431
1416543_at	2.4	4.97×10^{-11}	NRF2	25	1216	208	20265	15.0	1.7	2.7	0.0079708
1447849_s_at	−1.7	0.001631	c-Maf	11	1216	84	21012	4.9	2.3	2.9	0.0089414
1448797_at	1.9	0.000010	Elk-3	5	1216	23	21012	1.3	3.8	3.3	0.0090374
1447655_x_at	1.5	0.000477	SOX6	9	1216	63	21012	3.6	2.5	2.9	0.0099765
129Sv-SOD1^{G93A}											
1418747_at	1.5	0.014261	PU.1	79	1759	445	21012	37.3	2.1	7.2	1.158×10^{-10}
1417065_at	1.6	0.001171	EGR1	97	1759	737	21012	61.7	1.6	4.8	5.104×10^{-06}
1455267_at	−1.6	0.000072	ERR3	26	1759	121	21012	10.1	2.6	5.2	6.388×10^{-06}
1426031_a_at	−1.8	0.011070	NF-AT1(NFATC2)	25	1759	138	21012	11.6	2.2	4.1	0.0001856
1448452_at	6.9	1.454×10^{-15}	IRF8	24	1759	133	21012	11.1	2.2	4.0	0.0002628
1418982_at	1.6	0.003880	C/EBPalpha	66	1759	545	21012	45.6	1.4	3.2	0.0015174
1423100_at	1.6	0.003595	c-Fos	62	1759	511	21012	42.8	1.4	3.1	0.0019796
1459961_a_at	2.0	0.001566	STAT3	76	1759	660	21012	55.3	1.4	3.0	0.0027669
1449363_at	29.8	1.00 × 10−24	ATF-3	13	682	114	20265	3.8	3.4	4.8	0.0001211

[a]A network object ID corresponding to the given gene.
[b]Fold-change: expressed as mean fold-change ratio between four SOD1^{G93A} and four non-transgenic mice.
[c]Multiple hypothesis testing: Q-value[i] = mean (1-PPLR[1:i]) where PPLR is the probability of positive log ratio.
[d]Network object name in MetaBase™.
[e]Number of targets in the activated data set(s) regulated by the chosen transcription factor.
[f]Number of network objects in the activated data set(s).
[g]Number of targets in the complete database or background list regulated by the chosen transcription factor.
[h]Total number of gene-based objects in the complete database or background list.
[i]Mean value for hypergeometric distribution (n × R/N).
[j]Connectivity ratio (actual/expected).
[k]Z-score [(actual − expected)/sqrt(variance)].
[l]Probability to have the given value of actual or higher (or lower for negative *Z*-score).

models of rheumatoid arthritis and multiple sclerosis (Wallace *et al*., 1999; Wahl and Wallace, 2001; Weiss *et al*., 2006). Microglia are considered to be the major producer of oncostatin M in the CNS, although it is also expressed in neurons and astrocytes (Chen *et al*., 2006). The higher levels of *Osmr* in C57-SOD1^{G93A} compared with 129Sv-SOD1^{G93A} mice may be related to the lower levels of *Socs3* in the C57-SOD1^{G93A} strain. SOCS3 is known to inhibit the activation of JAK-STAT pathway by interacting with the OSMR subunit, gp130, and therefore reducing its levels of expression (Baker *et al*., 2009). Our data suggest that oncostatin M expression may drive a neuroprotective effect in motor neurons by influencing the expression pattern of *Serpina3n* (neuroserpin) and *Timp1* that are upregulated in C57-SOD1^{G93A} compared with 129Sv-SOD1^{G93A} motor neurons. TIMP1 has been described to be induced by oncostatin M in other cell systems and also to produce a neuroprotective effect by influencing the activity

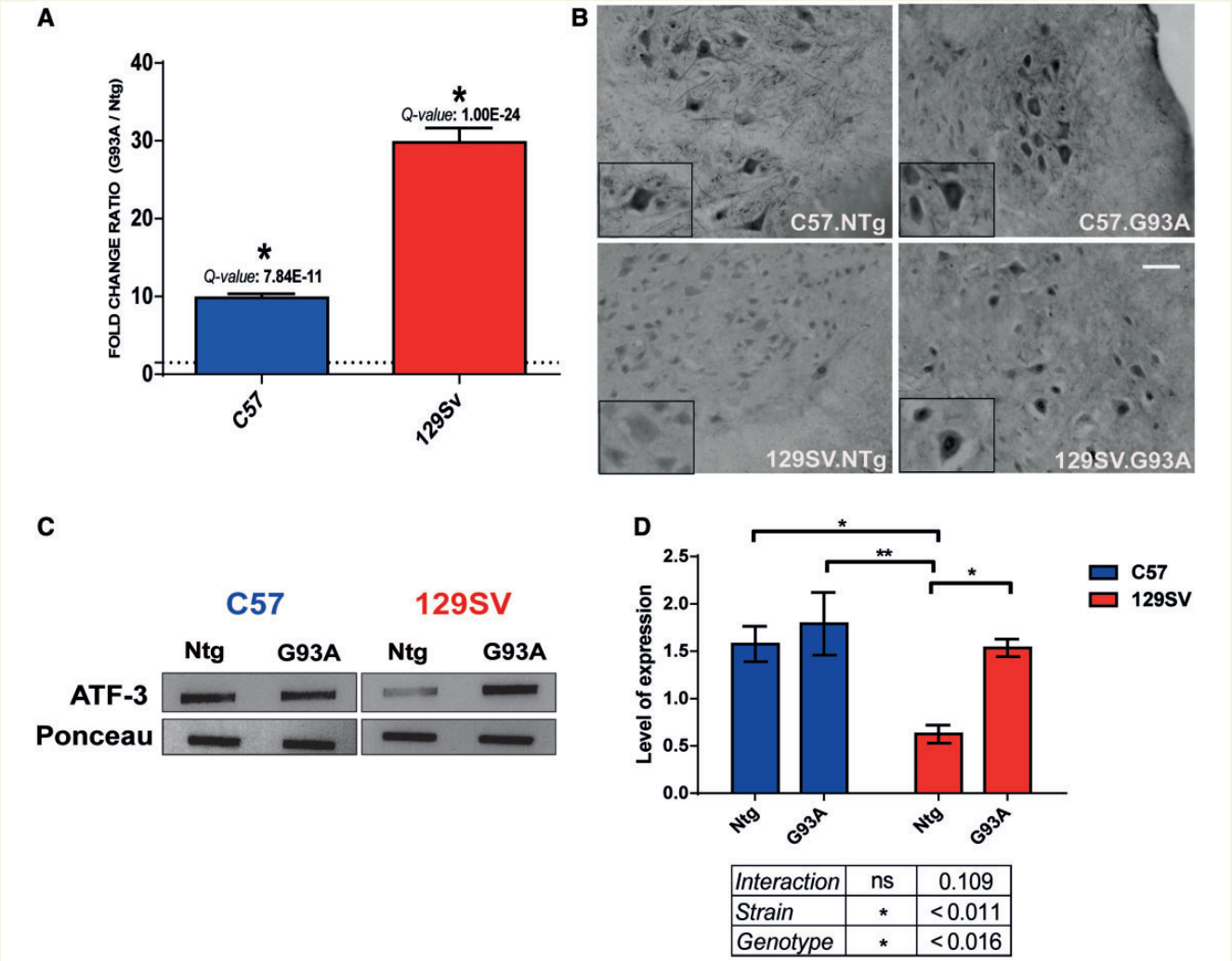

Figure 9 Analysis of ATF3 expression at disease onset. (**A**) *Atf3* messenger RNA levels are consistently higher in the 129Sv-SOD1^{G93A} (fold-change = 29.8) versus C57-SOD1^{G93A} (fold-change = 9.8) motor neurons. Messenger RNA levels are reported as mean fold change ratio (±SE) between SOD1^{G93A} ($n = 4$) and non-transgenic ($n = 4$) mice in 129Sv-SOD1^{G93A} and C57-SOD1^{G93A} motor neurons (dotted line defines the fold-change of 1.5). *Q*-values were generated from PPLR using the following formula: *Q-val*[i] = mean (1 − PPLR[1:i]); *Q-value ⩽ 0.01; ns = not significant. (**B**) Immunohistochemical comparison performed at disease onset on lumbar spinal cord of C57-SOD1^{G93A}, 129Sv-SOD1^{G93A} and non-transgenic littermates showing: (i) the expression of ATF3 by motor neurons; (ii) lower basal levels of ATF3 in 129sv-Ntg compared with C57-Ntg mice; (iii) a strong increase of ATF3 in 129Sv-SOD1^{G93A} versus their non-transgenic littermates; and (iv) no significant increase in ATF3 protein levels within C57-SOD1^{G93A} versus non-transgenic littermates. Scale bar = 20 μm. (**C**) ATF3 slot-blot analysis on longitudinally dissected lumbar ventral spinal cord extracts from C57-SOD1^{G93A}, 129Sv-SOD1^{G93A} and non-transgenic littermates at disease onset. Immunoreactivity was normalized to the actual amount of protein loaded on the membrane as detected after Red Ponceau (Fluka). (**D**) Densitometric analysis of ATF3 levels confirm the immunohistochemical findings. Data are reported as mean ± SE of four mice per group. Two-way statistical analysis shows the effect of strain (129Sv; C57 − F = 8.95) and the genotype (non-transgenic; G93A − F = 7.75) on the overall variability. Tukey's *post hoc* *$P < 0.05$; **$P < 0.01$.

of matrix metalloproteases (*Mmp-2* and *Mmp-9*) (Tong *et al.*, 2004; Weiss *et al.*, 2005; Chen *et al.*, 2006). Neuroserpin, on the other hand, inhibits the activity of tissue-type plasminogen activator (t-PA), a serine protease that is a major modulator of the excitotoxic cascade (Yepes *et al.*, 2000). In addition, the specific activation of *Stat1* may be responsible for the higher *Mcp-5* expression by C57-SOD1^{G93A} motor neurons (Fulkerson *et al.*, 2004; Kok *et al.*, 2009). *Mcp-5* is a mouse CC chemokine that is structurally and functionally homologous to of human MCP1 (Sarafi *et al.*, 1997). MCP1 (now known as CCL2) enhances trafficking of monocytes and T cells in the CNS (Huang *et al.*, 2001) and might represent the 'unknown' signal produced by injured motor neurons in order to attract T helper 2 and regulatory T cells into the spinal cord and maintain neuroprotective M2 microglia during the early stages of ALS (Appel *et al.*, 2010). Increased levels of human MCP1 have been reported in the serum, CSF and spinal cord (motor neurons and glial cells) of patients with ALS (Henkel *et al.*, 2004; Baron *et al.*, 2005; Tanaka *et al.*, 2006;

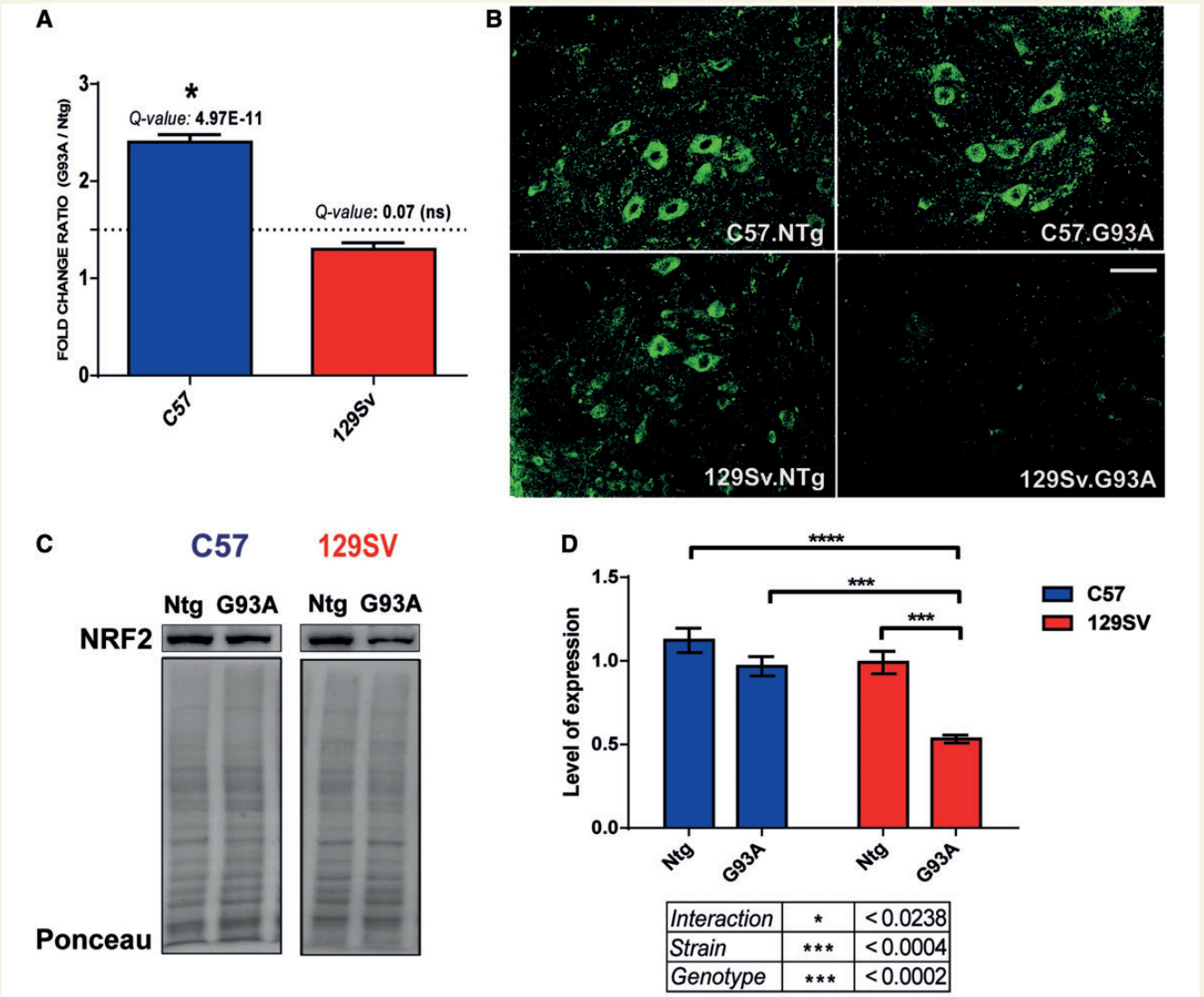

Figure 10 Analysis of NRF2 expression at disease onset. (**A**) *Nrf2* messenger RNA expression levels specifically increase in C57-SOD1^{G93A} motor neurons (fold change = 2.4). Messenger RNA levels are reported as mean fold-change ratio (±SE) between SOD1^{G93A} (n = 4) and non-transgenic (n = 4) mice in 129Sv-SOD1^{G93A} and C57-SOD1^{G93A} motor neurons (dotted line defines the fold-change of 1.5). Q-values were generated from PPLR using the following formula: *Q-val*[i] = mean (1 − PPLR[1:i]); *Q-value ⩽ 0.01; ns = not significant. (**B**) Immunohistochemical comparison performed at disease onset on lumbar spinal cord of C57-SOD1^{G93A}, 129Sv-SOD1^{G93A} and non-transgenic littermates showing: (i) the expression of NRF2 by motor neurons; and (ii) lower levels of NRF2 in 129Sv-SOD1^{G93A} motor neurons. Scale bar = 50 μm. (**C**) NRF2 western blot analysis on longitudinally dissected lumbar ventral spinal cord protein extracts from C57-SOD1^{G93A} 129Sv-SOD1^{G93A} and non-transgenic littermates at the onset of the disease. Immunoreactivity was normalized to the actual amount of proteins loaded on the membrane as detected after Red Ponceau (Fluka). (**D**) Densitometric analysis of NRF2 levels validates the immunohistochemical findings. Data are reported as mean ± SE of four mice per group. Two-way statistical analysis shows significant interaction (F int. = 6.69) due to strain (129Sv; C57 − F = 23.56) and genotype (non-transgenic; G93A − F = 27.45). Tukey's *post hoc* ***$P < 0.001$; ****$P < 0.0001$.

Nagata *et al.*, 2007). Previous studies reported increased messenger RNA levels of the putative murine homologue of human *MCP1*, *JE*, in the spinal cord and sciatic nerve homogenates from the mSOD1 mouse model of ALS (Henkel *et al.*, 2006; Chiu *et al.*, 2009). Unexpectedly, we did not find increased levels of JE messenger RNA in the ALS motor neurons analysed in the present study. These discrepant results may be related to the specificity of tissue analysed (motor neurons versus whole tissue homogenates). It is noteworthy, however, that from sequence analysis Mcp-5 is structurally more similar to human MCP1 than JE. In fact, the mature human MCP1 protein is 66% identical to the mature murine MCP-5 protein but only 55% identical to murine JE (Sarafi *et al.*, 1997).

In addition to *Mcp-5*, C57-SOD1^{G93A} motor neurons also show higher expression of other molecules involved in T cell/monocyte recruitment [chemokine (C-X-C motif) ligand 10] and activation

(*Cd22*, *Cd86*, *Cd48*, *Cd84*, *Cd44*) indicating that CNS immune cell infiltration and modulation may be higher in the spinal cord of slow progressing mice at disease onset and supporting the concept of a beneficial role of immune system activation on the early stages of disease progression (Chiu *et al.*, 2008; Beers *et al.*, 2008; Appel *et al.*, 2010; Beers *et al.*, 2011).

Motor neurons activate the complement system for their protection

We established that C57-SOD1^{G93A} motor neurons stimulate widespread complement activation through upregulation of the *C4b* and *C3* subunits. We were able to identify a higher level of expression of *C3* and *C3* activation products in C57-SOD1^{G93A} compared with 129Sv-SOD1^{G93A} motor neurons. Constitutive expression of proinflammatory complement components such as C3, C5, factor H and B was previously described in human neuronal cells *in vitro* and in cortical neurons and cerebellar Purkinje neurons in normal murine brains (Thomas *et al.*, 2000; Yu *et al.*, 2002). Other authors reported upregulation of *C1q* messenger RNA and protein in motor neurons from transgenic ALS mice (Lobsiger *et al.*, 2007). Most importantly, C3 protein accumulation and C3 activation product deposition was observed in motor neuron somata, sciatic nerve and neuromuscular junction from SOD1^{G93A} mouse model at the symptomatic stage of disease (Heurich *et al.*, 2011). The complement cascade is classically considered as a detrimental proinflammatory process, so that the general conclusions of these previous reports portray complement activation as an important contributor to motor neuron injury.

Conversely, our data suggest a neuroprotective role of the complement pathway in motor neurons as it is strongly activated at disease onset in C57-SOD1^{G93A} motor neurons and therefore is associated with a more benign disease course. Our hypothesis is in accord with the recent suggestion that activation of complement plays an important role in neuronal survival and even in normal neuronal development (Yanamadala and Friedlander, 2010). *In vitro*, C1q improves neuronal viability and neurite outgrowth through the induction of NGF and NT-3 (Benoit and Tenner, 2011), whereas complement C3 deficiency leads to accelerated amyloid-β plaque deposition and neurodegeneration in amyloid precursor protein transgenic mice (Maier *et al.*, 2008). In addition, the activity of C3a was reported to be neuroprotective against *N*-methyl-D-aspartic acid excitotoxicity (van Beek *et al.*, 2001) and essential for neuronal development (Shinjyo *et al.*, 2009). Notably, both transgenic motor neurons overexpress the complement component 3a receptor 1 (*C3ar1*) whereas only C57-SOD1^{G93A} motor neurons upregulate the complement component receptor (*C5ar1*). The expression of C5AR1 in primary neurons and cultured neuroblastoma cells was reported to be neuroprotective against damage produced by excitotoxins and amyloid-β peptide toxicity (O'Barr *et al.*, 2001). Consistent with this, exogenous C5a administration protects neurons against glutamate mediated neurotoxicity *in vitro* and *in vivo* (Tocco *et al.*, 1997; Osaka *et al.*, 1999; Mukherjee *et al.*, 2001, 2008). Recently our understanding of the complement system has markedly evolved beyond its early recognition as a protein system merely detecting and tagging a pathogen for further clearance. It is now firmly established that complement detects a growing repertoire of distinct self and non-self danger signals and is instrumental in the initiation and further fine-tuning of adaptive immunity (Heeger and Kemper, 2012). It is likely that the constitutive synthesis of complement proteins by motor neurons reflects a requirement for a 'primed' system in order to instantly deal with pathophysiological processes in the spinal cord and according to our data C57-SOD1^{G93A} motor neurons but not 129Sv-SOD1^{G93A} motor neurons, are able to amplify and finely regulate this system during the early development of ALS pathology.

Increased major histocompatibility complex I expression by motor neurons: a potential role in neuroprotection of the axonal compartment

A large number of proteins that were first discovered in the immune system, have been now detected in the healthy, uninfected nervous system, raising the possibility that these proteins have pleiotropic functions in the CNS (Boulanger *et al.*, 2001). Examples of immune molecules expressed by motor neurons include the MHCI complex. Rat spinal motor neurons constitutively express messenger RNAs for *MhcI* and β_2m (Lindå *et al.*, 1998) albeit at much lower levels that those found in tissues such as spleen and vascular endothelial cells. However, if motor neurons are exposed to injurious stimuli, such as axotomy, ventral-horn root avulsion, viral or parasitic infection or exposure to cytokines (Boulanger and Shatz, 2004), MHCI expression markedly increases. In the present study, we observed an increase of *MhcI* transcripts in the motor neurons of C57-SOD1^{G93A} at the onset of the disease, suggesting a potential neuroprotective role of this phenomenon. It is noteworthy that the increase of *MhcI* transcripts in motor neurons was associated with an increase in MHCI immunoreactivity in the motor axons and neuromuscular junction rather than in the perikarya, suggesting that this protein is rapidly transported away from the cell body. This finding is not surprising as other reports highlight the absence of MHCI-immunoreactivity in motor neuron somata after axotomy or in the experimental allergic encephalomyelitis (EAE) mouse model despite an upregulation of *MhcI* messenger RNA expression in the motor neuron cell bodies (Thams *et al.*, 2009; Freria *et al.*, 2010). Similar to our results, MHCI immunoreactivity was instead highly upregulated in the axonal compartment in the C57-SOD1^{G93A} mouse model after axotomy (Thams *et al.*, 2009). Recent studies highlight the importance of MHCI overexpression in axonal regeneration and the stability of the neuromuscular junctions of motor neurons after axonal damage (Oliveira *et al.*, 2004; Thams *et al.*, 2009). Therefore, the higher level of MHCI in C57-SOD1^{G93A} motor axons suggests a beneficial role of MHCI in preserving axonal integrity during the early phase of disease development in ALS.

Anterograde axonal transport of MHCI has been previously described in other neurons including the vomeronasal system *in vivo* and cortical and hippocampal neurons *in vitro* (Medana *et al.*, 2001; Ishii and Mombaerts, 2008; Taylor *et al.*, 2009).

Interestingly, these and other studies suggested an important role for MHCI in the refinement of synapse formation and plasticity in the visual system and the hippocampus (Corriveau *et al.*, 1998; Huh *et al.*, 2000; Boulanger and Shatz, 2004; Shatz, 2009). Thus, the remarkable overexpression of MHCI in the motor axons and neuromuscular junction at disease onset in C57 SOD1^{G93A} mice might explain the slowing of disease progression observed in this mouse strain compared to the 129Sv-SOD1^{G93A} strain. There is growing evidence indicating that distal axonopathy and retraction of the motor axon terminal from the muscle end plate is an early change in the pathophysiology of ALS (Fischer *et al.*, 2004; Dadon-Nachum *et al.*, 2011). The rapid induction of MHCI expression in motor axons may be an early neuroprotective response to neuromuscular junction dysfunction. Further investigation is required to identify the specific molecular mechanisms responsible for upregulation of MHCI expression by motor neurons.

Understanding the specific role of MHCI in the CNS will elucidate new aspects of CNS/immune system cross-talk and may provide a new target for therapeutic intervention to preserve axonal integrity. To date, no data have been published relating to the role of MHCI in ALS despite the report that ALS shows genetic linkage to the MHC coding region (Antel *et al.*, 1976; Kott *et al.*, 1979; Tiwari and Terasaki, 1985).

In parallel with an increase of MHCI expression, the present analysis reports the specific upregulation of *Lmp7* and *Psm1* in C57-SOD1^{G93A} motor neurons at disease onset time point. LMP7 and PSM1 are subcomponents of the immunoproteasome involved in antigen processing and presentation through the MHCI complex (Muchamuel *et al.*, 2009; de Graaf *et al.*, 2011). These results are in accordance with our previously published data showing altered levels of immunoproteasome subunits, including *Lmp7*, in C57-SOD1^{G93A} motor neurons during the early stage of disease (Cheroni *et al.*, 2009; Bendotti *et al.*, 2012). Here, we demonstrate that alterations of the immunoproteasome are probably related to an attempt by motor neurons to protect themselves from degeneration rather than having a role in the pathogenesis of the disease.

Defective levels of neuroprotective factors exacerbates the speed of disease progression in 129Sv-SOD1^{G93A} motor neurons

The systems biology analysis performed on data sets from both transgenic mice allows us to investigate specific key factors whose activity has been widely described as protective for motor neurons. In particular, the less severe ALS disease phenotype encountered in the transgenic C57 background is likely to be related to the specific ability of these mice to maintain the functional activity of certain key protein regulators. We observed that ANG is constitutively overexpressed in the C57 mouse strain compared with the 129Sv background. In addition, *Ang* messenger RNA upregulation in C57-SOD1^{G93A} motor neurons from the onset of disease seems to act to maintain (or reinstate) normal levels of the ANG protein inside the cell. In contrast, 129Sv-SOD1^{G93A} mice with the more aggressive disease course fail to upregulate *Ang* messenger RNA, with a concomitant dramatic reduction in ANG protein expression at disease onset. ANG was recently described to promote motor neuron survival *in vitro* and to have beneficial effects on the disease course in SOD1^{G93A} mice (Kieran *et al.*, 2008; Sebastià *et al.*, 2009; Li and Hu, 2010). Angiogenic activity of ANG is classically related to its ability to regulate ribosomal RNA transcription after nuclear translocation (Li and Hu, 2010; Aparicio-Erriu and Prehn, 2012) and motor neurons actively produce and secrete ANG to induce RNA cleavage in astroglia (Aparicio-Erriu and Prehn, 2012; Skorupa *et al.*, 2012). ANG mutations identified in patients with ALS (fALS9) are associated with a functional loss of ANG activity due to impairment of ribonucleolysis, nuclear translocation, or both (Kishikawa *et al.*, 2008; Li and Hu, 2010; Aparicio-Erriu and Prehn, 2012). In addition, decreased ANG levels were observed in the spinal cord of SOD1^{G93A} mice and ALS patients (Hu and Kishikawa, 2011) so that the downregulation of this protein in 129Sv-SOD1^{G93A} motor neurons at the onset of the disease may be interpreted as having a detrimental influence on disease progression.

Interestingly, NRF2 exhibits a pattern of expression similar to that observed for ANG where messenger RNA upregulation within C57-SOD1^{G93A} motor neurons underpins maintenance of normal levels of the NRF2 protein at the onset of the disease, whereas the lack of messenger RNA upregulation leads to reduced NRF2 protein expression in 129Sv-SOD1^{G93A} motor neurons. The NF-E2-related factor 2/antioxidant response element (Nrf2/antioxidant response element) signalling programme is an endogenous cytoprotective system that is ubiquitously expressed (Barber and Shaw, 2010; Jung and Kwak, 2010). The activation of NRF2 promotes expression of an array of neuroprotective proteins including those involved in glutathione biosynthesis, and antioxidant defence and phase II drug metabolizing enzymes. This system has been shown to be effective at blocking neurotoxicity *in vitro* and *in vivo*. (Lee *et al.*, 2003; Shih *et al.*, 2003; Kraft *et al.*, 2004, 2006; Mead *et al.*, 2013). Dysregulation of NRF2 and the antioxidant response element has been reported in an NSC34 cellular model of SOD1-associated familial ALS (Kirby *et al.*, 2005) as well as in the motor cortex and spinal cord of patients with ALS (Sarlette *et al.*, 2008). Induction of NRF2 overexpression in the spinal cord (motor neurons and astrocytes) and distal muscle of SOD1 transgenic ALS mice model showed neuroprotective effects (Kraft *et al.*, 2007; Vargas *et al.*, 2008). Thus, impairment of the Nrf2/antioxidant response element signalling system appears to increase the vulnerability of motor neurons to stress-induced toxic insults.

Increased expression levels of ANG and NRF2 observed in C57-SOD1^{G93A} motor neurons at disease onset appear to be key factors involved in slowing disease progression. In contrast, motor neurons from the rapid progressor 129Sv-SOD1^{G93A} strain appear to lack an equivalent robust ANG and NRF2 motor neuronal stress response.

Impairment of key functions at disease onset in the motor neurons from 129Sv-SOD1^{G93A} mice

According to our microarray data, the dysregulation of key neuroprotective factors within 129Sv-SOD1^{G93A} motor neurons may

be the consequence of a multisystem impairment involving different compartments and cellular processes. The increased state of stress of motor neurons from the 129Sv-SOD1^{G93A} strain was confirmed by monitoring ATF3 levels during the progression of the disease. ATF3, which is strongly overexpressed in 129Sv-SOD1^{G93A} mice versus 129Sv non-transgenic littermates at disease onset, is a member of the ATF/CREB family of transcription factors whose upregulation is directly proportional to motor neuron impairment and axonal injury (Tsujino *et al.*, 2000; Vlug *et al.*, 2005). The 129Sv-SOD1^{G93A} motor neuron gene signature predicts that three vital biological processes are strikingly compromised at disease onset: energy metabolism; protein degradation and vesicle trafficking.

Mitochondria from the rapid progressor mouse strain show a widespread downregulation of messenger RNAs encoding Krebb's cycle enzymes, the NADH dehydrogenase complex and ATP synthase. The gene expression data were validated by the demonstration of a dramatic decrease in the activity of the electronic transport chain complex I and ATP production in the ventral spinal cord of 129Sv-SOD1^{G93A} mice. Although functional alterations of mitochondria related to an increase in oxidative stress and exitotoxicity have been widely reported in the context of ALS (Shi *et al.*, 2010; Duffy *et al.*, 2011; Cozzolino *et al*., 2012; Federico *et al.*, 2012; Johri and Beal, 2012), the order of events leading to mitochondrial dysfunction is far from clear. Our data highlight the dysregulation of two mechanisms potentially involved in mitochondrial stability: the massive downregulation of the mitochondrial translational machinery and the upregulation of the uncoupling protein 2. Both of these mechanisms have been reported to be protective against oxidative stress, decreasing the redox pressure on the electronic transport chain (Crawford *et al.*, 1997; Kristal *et al.*, 1997; Dulloo *et al.*, 2001; Serviddio *et al.*, 2008). However, their induction in pathological conditions may result in a dramatic decrease in the efficiency of ATP production, as well as the induction of a form of cell death that morphologically resembles oncosis (Mills *et al.*, 2002).

Proteasome alterations related to protein aggregation have been widely reported in transgenic ALS mouse models and are now considered as one of the main hallmarks of the disease (Bendotti *et al.*, 2012). The present microarray analysis predicts a defect of the ubiquitin proteasome system in 129Sv-SOD1^{G93A} motor neurons from disease onset. ATF3 protein overexpression in 129Sv motor neurons represents an index of a gradual intracellular accumulation of ubiquitinated material in motor neurons (Vlug *et al.*, 2005). Interestingly, ATF3 has recently been reported as a novel repressor of NRF2 (Brown *et al.*, 2008) so that higher levels of ATF3 may cause reduced expression of NRF2 that, in turn, may affect proteasome composition and stability (Kapeta *et al.*, 2010; Pickering *et al.*, 2010, 2012). In addition, through the analysis of expression levels of UCH37, we propose a novel mechanism that may be responsible for improper processing of unfolded proteins. The proteasome generally recognizes substrate through its multi-ubiquitin chain, followed by ATP-dependent unfolding and translocation of the substrate from the regulatory particle into the proteolytic core particle to be degraded. Substrate-bound ubiquitin groups are for the most part not delivered to the core particle and broken down together with substrate, but instead recovered as intact free ubiquitin and ubiquitin chains. UCH37, together with 26S proteasome regulatory subunit RPN11 and ubiquitin carboxyl-terminal hydrolase 14, is responsible for the deubiquitination of the substrate on the proteasome (Qiu *et al.*, 2006; Yao *et al.*, 2006). Reduced levels of UCH37 in 129Sv-SOD1^{G93A} motor neurons may therefore be responsible, in addition to proteasome alterations, for the increased formation of cytosolic poly-ubiquitinated unfolded protein inclusions found in these mice as compared to the C57-SOD1^{G93A} mice (in press).

A further noteworthy finding is that the dysregulation of the vesicle-associated membrane protein-associated protein B and C, chromatin modifying protein 2B, together with 21 other SNAREs and GTPase proteins, in 129Sv-SOD1^{G93A} motor neurons. This depicts a complex scenario in which the malfunctioning of an intricate protein-network may affect motor neuron physiology. In recent years, an increasing number of mutations have been identified in genomic sequences of transgenic mice and ALS patients coding for different proteins involved in vesicle trafficking and protein targeting (Schmitt-John *et al.*, 2005; Parkinson *et al.*, 2006; Teuling *et al.*, 2007; Cox *et al.*, 2010). Among these, vesicle-associated membrane protein-associated protein B and C, is normally activated when misfolded proteins accumulate in the endoplasmic reticulum, and when mutated it promotes ubiquitinated aggregate formation and neuronal cell death. Similarly, mutation of proteins that regulate protein sorting to the endosome including chromatin modifying protein 2B and vacuolar protein sorting 24 are associated with motor neuron injury. Vesicle trafficking is an essential cellular function that regulates the homeostasis of subcellular compartments as well as the normal activity of physiological processes such as autophagy and neurotransmitter release (Jahn and Scheller, 2006; Chaineau *et al.*, 2009; Longatti *et al.*, 2009; Sann *et al.*, 2009; Santos *et al.*, 2009). In addition, recent findings have begun to provide a more detailed view of the molecular mechanisms underlying vesicle trafficking in neuronal cells. Trafficking through the Golgi is required for dendritic growth, whereas endosomal trafficking regulates neurite outgrowth and guidance (Sann *et al.*, 2009). For example, disrupting the function of vesicle-associated membrane protein 7 prevents outgrowth of both axons and dendrites in mouse hippocampal neurons (Martinez-Arca *et al.*, 2001) whereas loss of vacuolar protein sorting 35 causes signalling defects at the neuromuscular junction, including upregulation of TGF-β/BMP signalling and excessive formation of synaptic terminals (Korolchuk *et al.*, 2007). Thus, downregulated expression of this cluster of genes in the 129Sv-SOD1^{G93A} motor neurons at the onset of disease may predispose the mice to rapid disease progression.

The last two gene categories specifically downregulated at disease onset in 129Sv-SOD1^{G93A} motor neurons are involved in microtubule stability and neuron projections. Interestingly, the gene cluster analysis reports downregulation of messenger RNAs encoding two non-catalytic subunits of dynein 1 complex, six kinesin heavy chain isoforms and one kinesin light chain isoform. Amongst these, *Kif5a*, *Kif5b* and *Kif5c* are expressed at high levels in normal adult motor neurons (Kanai *et al.* 2000) and are involved in neurofilament and mitochondrial axonal transport (Xia *et al*., 2003; Cho *et al*., 2007). The analysis of protein levels reveals that KIF5A, KIF5B and KIF5C are markedly reduced

in 129Sv-SOD1^{G93A} mice, at disease onset. These results predict that anterograde axonal transport is likely to be impaired in motor neurons from the rapidly progressing mice from the initial phase of the disease.

Impairment of axonal transport has been reported in multiple neurodegenerative diseases, including ALS (De Vos *et al*., 2008; Magrané and Manfredi, 2009; Bilsland *et al.*, 2010; Millecamps and Julien, 2013). Deficits in bidirectional motor axonal transport have been documented in SOD1^{G93A} mice even at the presymptomatic stage of the disease, suggesting that this phenomenon represents an early pathophysiological index of motor neuron impairment (Bilsland *et al.*, 2010). It has been reported that axonal transport is in turn strongly influenced by mitochondrial activity and it has been proposed that loss of mitochondrial membrane potential is associated with an increase in retrograde transport (Miller and Sheetz, 2004). These findings have been confirmed in cultured motor neurons from SOD1^{G93A} mice where mitochondrial transport is reduced in the anterograde direction, resulting in 50% depletion in the number of mitochondria in axons (De Vos *et al.*, 2007). Thus, it is likely that the massive deficit in mitochondrial activity demonstrated in 129Sv-SOD1^{G93A} motor neurons, coupled with impairment of axonal transport, might influence motor neuron homeostasis at disease onset underpinning a more rapid disease progression in these mice compared to the C57SOD1^{G93A} mice.

Conclusion

Evidence from genetically engineered SOD1 transgenic mice suggests that the onset of the disease involves incompletely characterized processes in motor neurons, whereas disease progression after onset involves microglia, astrocytes and the blood–brain barrier (Boillee *et al.*, 2006*a*, *b*; Maragakis and Rothstein, 2006; Lobsiger *et al.*, 2007; Jaarsma *et al.*, 2008; Yamanak *et al.*, 2008; Zhong *et al.*, 2008). Consistent with this notion, our longitudinal gene expression analysis of motor neurons provides evidence that specific alterations occurring in motor neurons at disease onset are fundamental in dictating the subsequent course of the disease. In particular, the capacity of motor neurons to activate immunological, angiogenic and anti-oxidative processes seems to promote neuroprotective effects that are associated with slower disease progression. In contrast, when these mechanisms are less robustly activated as in the 129Sv-SOD1^{G93A} mice, a massive impairment of mitochondrial function and protein catabolic processes ensues associated with a more aggressive disease course. Given the complexity of the genes that are differentially expressed in the motor neurons of these two transgenic mouse models, it is difficult to extrapolate a single target for the development of effective therapies. However, this study has identified a set of key genes and pathways that are likely to account for the severity of the disease course in murine ALS and which may prove useful in unravelling the heterogeneity of the human disease. Currently, there is striking evidence that genetic modifiers identified in transgenic mice may represent important candidates underlying the disease phenotype in humans (Van Hoecke *et al.*, 2012). Identification of genetically controlled indices of fast and slow disease progression in human ALS could lead to several translational benefits including elucidation of biomarkers for better disease stratification and therapeutic strategies to upregulate molecular factors determining slower disease progression.

Finally, our results add weight to the recent evidence suggesting a beneficial role of the inflammatory response on the progression of ALS (Beers *et al.*, 2008, 2011; Chiu *et al.*, 2008; Appel *et al.*, 2010) as the mouse strain with the slower disease course shows more significant activation of immunological pathways at the time of disease onset. Major attention has been given to astrocytes, microglia, oligodendrocytes and most recently to the immune system as important players in the modulation of the disease course in ALS.

In this report, we highlight the propensity of motor neurons to activate immunological defence mechanisms as well as other protective mechanisms, in response to cell stress induced by the presence of mutant SOD1. The genetic background of the SOD1 mutant mouse has a large influence on the balance of these pathways and, as a consequence, on the rapidity of the disease course and lifespan of the animals. Detailed understanding of these pathways in human patients with ALS may provide new targets for therapies to ameliorate disease progression.

Funding

This work was supported by the Motor Neurone Disease Association (Grant number 124695-1), Regione Lombardia under Institutional Agreement no. 14501A and from the European Community's Seventh Frame Work Programme (FP7 / 2007-2013) under grant agreement n° (259867 - Euromotor). P.J.S. is supported by NIHR as a Senior Investigator.

Supplementary material

Supplementary material is available at *Brain* online.

References

Adalbert R, Coleman MP. Axon pathology in age-related neurodegenerativedis orders. Neuropathol Appl Neurobiol 2013; 39: 90–108.

Antel JP, Arnason BG, Fuller TC, Lehrich JR. Histocompatibility typing in amyotrophic lateral sclerosis. Arch Neurol 1976; 33: 423–5.

Aparicio-Erriu IM, Prehn JH. Molecular mechanisms in amyotrophic lateral sclerosis: the role of angiogenin, a secreted RNase. Front Neurosci 2012; 6: 167.

Appel SH, Beers DR, Henkel JS. T cell-microglial dialogue in Parkinson's disease and amyotrophic lateral sclerosis: are we listening? Trends Immunol 2010; 31: 7–17.

Ashley C, Pastushok L, McKenna S, Ellison MJ, Xiao W. Roles of mouse UBC13 in DNA postreplication repair and Lys63-linked ubiquitination. Gene 2002; 285: 183–91.

Baker BJ, Akhtar LN, Benveniste EN. SOCS1 and SOCS3 in the control of CNS immunity. Trends Immunol 2009; 30: 392–400.

Barber SC, Shaw PJ. Oxidative stress in ALS: key role in motor neuron injury and therapeutic target. Free Radic Biol Med 2010; 48: 629–41.

Baron P, Bussini S, Cardin V, Corbo M, Conti G, Galimberti D, et al. Production of monocyte chemoattractant protein-1 in amyotrophic lateral sclerosis. Muscle Nerve 2005; 32: 541–4.

Basso M, Samengo G, Nardo G, Massignan T, D'Alessandro G, Tartari S, et al. Characterization of detergent-insoluble proteins in ALS indicates a causal link between nitrative stress and aggregation in pathogenesis. PLoS One 2009; 4: e8130.

Beers DR, Henkel JS, Zhao W, Wang J, Appel SH. CD4+ T cells support glial neuroprotection, slow disease progression, and modify glial morphology in an animal model of inherited ALS. Proc Natl Acad Sci USA 2008; 105: 15558–63.

Beers DR, Henkel JS, Zhao W, Wang J, Huang A, Wen S, et al. Endogenous regulatory T lymphocytes ameliorate amyotrophic lateral sclerosis in mice and correlate with disease progression in patients with amyotrophic lateral sclerosis. Brain 2011; 134: 1293–314.

Beghi E, Mennini T, Bendotti C, Bigini P, Logroscino G, Chiò A, et al. The heterogeneity of amyotrophic lateral sclerosis: a possible explanation of treatment failure. Curr Med Chem 2007; 14: 3185–200.

Bendotti C, Carrì MT. Lessons from models of SOD1-linked familial ALS. Trends Mol Med 2004; 10: 393–400.

Bendotti C, Marino M, Cheroni C, Fontana E, Crippa V, Poletti A, et al. Dysfunction of constitutive and inducible ubiquitin-proteasome system in amyotrophic lateral sclerosis: implication for protein aggregation and immune response. Prog Neurobiol 2012; 97: 101–26.

Benoit ME, Tenner AJ. Complement protein C1q-mediated neuroprotection is correlated with regulation of neuronal gene and microRNA expression. J Neurosci 2011; 31: 3459–69.

Bhosle RC, Michele DE, Campbell KP, Li Z, Robson RM. Interactions of intermediate filament protein synemin with dystrophin and utrophin. Biochem Biophys Res Commun 2006; 346: 768–77.

Bilsland LG, Sahai E, Kelly G, Golding M, Greensmith L, Schiavo G. Deficits in axonal transport precede ALS symptoms in vivo. Proc Natl Acad Sci USA 2010; 107: 20523–8.

Boillee S, Yamanaka K, Lobsiger CS, Copeland NG, Jenkins NA, Kassiotis G, et al. Onset and progression in inherited ALS determined by motor neurons and microglia. Science 2006a; 312: 1389–92.

Boillee S, Vande Velde C, Cleveland DW. ALS: a disease of motor neurons and their nonneuronal neighbors. Neuron 2006b; 52: 39–59.

Boulanger LM, Huh GS, Shatz CJ. Neuronal plasticity and cellular immunity: shared molecular mechanisms. Curr Opin Neurobiol 2001; 11: 568–78.

Boulanger LM, Shatz CJ. Immune signalling in neural development, synaptic plasticity and disease. Nat Rev Neurosci 2004; 5: 521–31.

Brown SL, Sekhar KR, Rachakonda G, Sasi S, Freeman ML. Activating transcription factor 3 is a novel repressor of the nuclear factor erythroid-derived 2-related factor 2 (Nrf2)-regulated stress pathway. Cancer Res 2008; 68: 364–8.

Carninci P, Kasukawa T, Katayama S, Gough J, Frith MC, Maeda N, et al. The transcriptional landscape of the mammalian genome. Science 2005; 309: 1559–63.

Chaineau M, Danglot L, Galli T. Multiple roles of the vesicular-SNARE TI-VAMP in post-Golgi and endosomal trafficking. FEBS Lett 2009; 583: 3817–26.

Chatterton JE, Hirsch D, Schwartz JJ, Bickel PE, Rosenberg RD, Lodish HF, et al. Expression cloning of LDLB, a gene essential for normal Golgi function and assembly of the ldlCp complex. Proc Natl Acad Sci USA 1999; 96: 915–20.

Chen HJ, Anagnostou G, Chai A, Withers J, Morris A, Adhikaree J, et al. Characterization of the properties of a novel mutation in VAPB in familial amyotrophic lateral sclerosis. J Biol Chem 2010; 285: 40266–81.

Chen SH, Benveniste EN. Oncostatin M: a pleiotropic cytokine in the central nervous system. Cytokine Growth Factor Rev 2004; 15: 379–91.

Chen SH, Gillespie GY, Benveniste EN. Divergent effects of oncostatin M on astroglioma cells: influence on cell proliferation, invasion, and expression of matrix metalloproteinases. Glia 2006; 53: 191–200.

Cheroni C, Marino M, Tortarolo M, Veglianese P, De Biasi S, Fontana E, et al. Functional alterations of the ubiquitin-proteasome system in motor neurons of a mouse model of familial amyotrophic lateral sclerosis. Hum Mol Genet 2009; 18: 82–96.

Chiu IM, Chen A, Zheng Y, Kosaras B, Tsiftsoglou SA, Vartanian TK, et al. T lymphocytes potentiate endogenous neuroprotective inflammation in a mouse model of ALS. Proc Natl Acad Sci USA 2008; 105: 17913–8.

Chiu IM, Phatnani H, Kuligowski M, Tapia JC, Carrasco MA, Zhang M, et al. Activation of innate and humoral immunity in the peripheral nervous system of ALS transgenic mice. Proc Natl Acad Sci USA 2009; 106: 20960–5.

Cho KI, Cai Y, Yi H, Yeh A, Aslanukov A, Ferreira PA. Association of the kinesin-binding domain of RanBP2 to KIF5B and KIF5C determines mitochondria localization and function. Traffic 2007; 8: 1722–35.

Cleveland DW, Rothstein JD. From Charcot to Lou Gehrig: deciphering selective motor neuron death in ALS. Nat Rev Neurosci 2001; 2: 806–19.

Cooper-Knock J, Kirby J, Ferraiuolo L, Heath PR, Rattray M, Shaw PJ. Gene expression profiling in human neurodegenerative disease. Nat Rev Neurol 2012; 8: 518–30.

Corriveau RA, Huh GS, Shatz CJ. Regulation of class I MHC gene expression in the developing and mature CNS by neural activity. Neuron 1998; 21: 505–20.

Cox LE, Ferraiuolo L, Goodall EF, Heath PR, Higginbottom A, Mortiboys H, et al. Mutations in CHMP2B in lower motor neuron predominant amyotrophic lateral sclerosis (ALS). PLoS One 2010; 5: e9872.

Cozzolino M, Pesaresi MG, Gerbino V, Grosskreutz J, Carrì MT. Amyotrophic lateral sclerosis: new insights into underlying molecular mechanisms and opportunities for therapeutic intervention. Antioxid Redox Signal 2012; 17: 1277–330.

Crawford DR, Wang Y, Schools GP, Kochheiser J, Davies KJ. Down-regulation of mammalian mitochondrial RNAs during oxidative stress. Free Radic Biol Med 1997; 22: 551–9.

Dadon-Nachum M, Melamed E, Offen D. The "dying-back" phenomenon of motor neurons in ALS. J Mol Neurosci 2011; 43: 470–7.

de Graaf N, van Helden MJ, Textoris-Taube K, Chiba T, Topham DJ, Kloetzel PM, et al. PA28 and the proteasome immunosubunits play a central and independent role in the production of MHC class I-binding peptides in vivo. Eur J Immunol 2011; 41: 926–35.

Denarier E, Fourest-Lieuvin A, Bosc C, Pirollet F, Chapel A, Margolis RL, et al. Nonneuronal isoforms of STOP protein are responsible for microtubule cold stability in mammalian fibroblasts. Proc Natl Acad Sci USA 1998; 95: 6055–60.

De Vos KJ, Chapman AL, Tennant ME, Manser C, Tudor EL, Lau KF, et al. Familial amyotrophic lateral sclerosis-linked SOD1 mutants perturb fast axonal transport to reduce axonal mitochondria content. Hum Mol Genet 2007; 16: 2720–8.

De Vos KJ, Grierson AJ, Ackerley S, Miller CC. Role of axonal transport in neurodegenerative diseases. Annu Rev Neurosci 2008; 31: 151–73.

Duffy LM, Chapman AL, Shaw PJ, Grierson AJ. The role of mitochondria in the pathogenesis of amyotrophic lateral sclerosis. Neuropathol Appl Neurobiol 2011; 37: 336–52.

Dulloo AG, Samec S. Uncoupling proteins: their roles in adaptive thermogenesis and substrate metabolism reconsidered. Br J Nutr 2001; 86: 123–39.

Edgar R, Domrachev M, Lash AE. Gene Expression Omnibus: NCBI gene expression and hybridization array data repository. Nucleic Acids Res 2002; 30: 207–10.

Ende N, Weinstein F, Chen R, Ende M. Human umbilical cord blood effect on sod mice (amyotrophic lateral sclerosis). Life Sci 2000; 67: 53–9.

Federico A, Cardaioli E, Da Pozzo P, Formichi P, Gallus GN, Radi E. Mitochondria, oxidative stress and neurodegeneration. J Neurol Sci 2012; 322: 254–62.

Ferraiuolo L, Heath PR, Holden H, Kasher P, Kirby J, Shaw PJ. Microarray analysis of the cellular pathways involved in the adaptation to and progression of motor neuron injury in the SOD1 G93A mouse model of familial ALS. J Neurosci 2007; 27: 9201–19.

Ferraiuolo L, Kirby J, Grierson AJ, Sendtner M, Shaw PJ. Molecular pathways of motor neuron injury in amyotrophic lateral sclerosis. Nat Rev Neurol 2011; 7: 616–30.

Fischer LR, Culver DG, Tennant P, Davis AA, Wang M, Castellano-Sanchez A, et al. Amyotrophic lateral sclerosis is a distal axonopathy: evidence in mice and man. Exp Neurol 2004; 185: 232–40.

Freria CM, Zanon RG, Santos LM, Oliveira AL. Major histocompatibility complex class I expression and glial reaction influence spinal motoneuron synaptic plasticity during the course of experimental autoimmune encephalomyelitis. J Comp Neurol 2010; 518: 990–1007.

Fulkerson PC, Zimmermann N, Hassman LM, Finkelman FD, Rothenberg ME. Pulmonary chemokine expression is coordinately regulated by STAT1, STAT6, and IFN-gamma. J Immunol 2004; 173: 7565–74.

Gentleman RC, Carey VJ, Bates DM, Bolstad B, Dettling M, Dudoit S, et al. Bioconductor: open software development for computational biology and bioinformatics. Genome Biol 2004; 5: R80.

Glass CK, Saijo K, Winner B, Marchetto MC, Gage FH. Mechanisms underlying inflammation in neurodegeneration. Cell 2010; 140: 918–34.

Gurney ME. Transgenic-mouse model of amyotrophic lateral sclerosis. N Engl J Med 1994; 331: 1721–2.

Heeger PS, Kemper C. Novel roles of complement in T effector cell regulation. Immunobiology 2012; 217: 216–24.

Heiman-Patterson TD, Deitch JS, Blankenhorn EP, Erwin KL, Perreault MJ, Alexander BK, et al. Background and gender effects on survival in the TgN(SOD1-G93A)1Gur mouse model of ALS. J Neurol Sci 2005; 236: 1–7.

Heiman-Patterson TD, Sher RB, Blankenhorn EA, Alexander G, Deitch JS, Kunst CB, et al. Effect of genetic background on phenotype variability in transgenic mouse models of amyotrophic lateral sclerosis: a window of opportunity in the search for genetic modifiers. Amyotroph Lateral Scler 2011; 12: 79–86.

Henkel JS, Engelhardt JI, Siklós L, Simpson EP, Kim SH, Pan T, et al. Presence of dendritic cells, MCP-1, and activated microglia/macrophages in amyotrophic lateral sclerosis spinal cord tissue. Ann Neurol 2004; 55: 221–35.

Henkel JS, Beers DR, Siklós L, Appel SH. The chemokine MCP-1 and the dendritic and myeloid cells it attracts are increased in the mSOD1 mouse model of ALS. Mol Cell Neurosci 2006; 31: 427–37.

Heurich B, El Idrissi NB, Donev RM, Petri S, Claus P, Neal J, et al. Complement upregulation and activation on motor neurons and neuromuscular junction in the SOD1 G93A mouse model of familial amyotrophic lateral sclerosis. J Neuroimmunol 2011; 235: 104–9.

Hu GF, Kishikawa H. Angiogenin and amyotrophic lateral sclerosis. United States Patent Application Publication. 2011. US 2011/0078804 A.

Huang DR, Wang J, Kivisakk P, Rollins BJ, Ransohoff RM. Absence of monocyte chemoattractant protein 1 in mice leads to decreased local macrophage recruitment and antigen-specific T helper cell type 1 immune response in experimental autoimmune encephalomyelitis. J Exp Med 2001; 193: 713–26.

Huang da W, Sherman BT, Lempicki RA. Systematic and integrative analysis of large gene lists using DAVID bioinformatics resources. Nat Protoc 2009; 4: 44–57.

Huh GS, Boulanger LM, Du H, Riquelme PA, Brotz TM, Shatz CJ. Functional requirement for class I MHC in CNS development and plasticity. Science 2000; 290: 2155–9.

Ishii T, Mombaerts P. Expression of nonclassical class I major histocompatibility genes defines a tripartite organization of the mouse vomeronasal system. J Neurosci 2008; 28: 2332–41.

Jaarsma D, Teuling E, Haasdijk ED, De Zeeuw CI, Hoogenraad CC. Neuronspecific expression of mutant superoxide dismutase is sufficient to induce amyotrophic lateral sclerosis in transgenic mice. J Neurosci 2008; 28: 2075–88.

Jahn R, Scheller RH. SNAREs–engines for membrane fusion. Nat Rev Mol Cell Biol 2006; 7: 631–43.

Jena BP. Role of SNAREs in membrane fusion. Adv Exp Med Biol 2011; 713: 13–32.

Johri A, Beal MF. Mitochondrial dysfunction in neurodegenerative diseases. J Pharmacol Exp Ther 2012; 342: 619–30.

Jung KA, Kwak MK. The Nrf2 system as a potential target for the development of indirect antioxidants. Molecules 2010; 15: 7266–91.

Jung C, Higgins CM, Xu Z. A quantitative histochemical assay for activities of mitochondrial electron transport chain complexes in mouse spinal cord sections. J Neurosci Methods 2002a; 114: 165–72.

Jung C, Higgins CM, Xu Z. Mitochondrial electron transport chain complex dysfunction in a transgenic mouse model for amyotrophic lateral sclerosis. J Neurochem 2002b; 83: 535–45.

Kanai Y, Okada Y, Tanaka Y, Harada A, Terada S, Hirokawa N. KIF5C, a novel neuronal kinesin enriched in motor neurons. J Neurosci 2000; 20: 6374–84.

Kapeta S, Chondrogianni N, Gonos EASE. Nuclear erythroid factor 2-mediated proteasome activation delays senescence in human fibroblasts. J Biol Chem 2010; 285: 8171–84.

Karras GI, Jentsch S. The RAD6 DNA damage tolerance pathway operates uncoupled from the replication fork and is functional beyond S phase. Cell 2010; 141: 255–67.

Kato S. Amyotrophic lateral sclerosis models and human neuropathology: similarities and differences. Acta Neuropathol 2008; 115: 97–114.

Kieran D, Sebastia J, Greenway MJ, King MA, Connaughton D, Concannon CG, et al. Control of motoneuron survival by angiogenin. J Neurosci 2008; 28: 14056–61.

Kirby J, Halligan E, Baptista MJ, Allen S, Heath PR, Holden H, et al. Mutant SOD1 alters the motor neuronal transcriptome: implications for familial ALS. Brain 2005; 128: 1686–706.

Kishikawa H, Wu D, Hu GF. Targeting angiogenin in therapy of amyotrophic lateral sclerosis. Expert Opin Ther Targets 2008; 12: 1229–42.

Kok SH, Hong CY, Kuo MY, Wang CC, Hou KL, Lin YT, et al. Oncostatin M-induced CCL2 transcription in osteoblastic cells is mediated by multiple levels of STAT-1 and STAT-3 signaling: an implication for the pathogenesis of arthritis. Arthritis Rheum 2009; 60: 1451–62.

Korolchuk VI, Schütz MM, Gómez-Llorente C, Rocha J, Lansu NR, Collins SM, et al. Drosophila Vps35 function is necessary for normal endocytic trafficking and actin cytoskeleton organisation. J Cell Sci 2007; 120: 4367–76.

Kott E, Kott E, Livni E, Zamir R, Kuritzky A. Cell-mediated immunity to polio and HLA antigens in amyotrophic lateral sclerosis. Neurology 1979; 29: 1040–4.

Kraft AD, Johnson DA, Johnson JA. Nuclear factor E2-related factor 2-dependent antioxidant response element activation by tert-butylhydroquinone and sulforaphane occurring preferentially in astrocytes conditions neurons against oxidative insult. J Neurosci 2004; 24: 1101–12.

Kraft AD, Lee JM, Johnson DA, Kan YW, Johnson JA. Neuronal sensitivity to kainic acid is dependent on the Nrf2-mediated actions of the antioxidant response element. J Neurochem 2006; 98: 1852–65.

Kraft AD, Resch JM, Johnson DA, Johnson JA. Activation of the Nrf2-ARE pathway in muscle and spinal cord during ALS-like pathology in mice expressing mutant SOD1. Exp Neurol 2007; 207: 107–17.

Kristal BS, Koopmans SJ, Jackson CT, Ikeno Y, Park BJ, Yu BP. Oxidant-mediated repression of mitochondrial transcription in diabetic rats. Free Radic Biol Med 1997; 22: 813–22.

Krumbholz M, Theil D, Cepok S, Hemmer B, Kivisäkk P, Ransohoff RM, et al. Chemokines in multiple sclerosis: CXCL12 and CXCL13 up-regulation is differentially linked to CNS immune cell recruitment. Brain 2006; 129: 200–11.

Lee JM, Shih AY, Murphy TH, Johnson JA. NF-E2-related factor-2 mediates neuroprotection against mitochondrial complex I inhibitors and increased concentrations of intracellular calcium in primary cortical neurons. J Biol Chem 2003; 278: 37948–56.

Lee MJ, Lee BH, Hanna J, King RW, Finley D. Trimming of ubiquitin chains by proteasome-associated deubiquitinating enzymes. Mol Cell Proteomics 2011; 10R110.003871.

Li S, Hu GF. Angiogenin-mediated rRNA transcription in cancer and neurodegeneration. Int J Biochem Mol Biol 2010; 1: 26–35.

Lindå H, Hammarberg H, Cullheim S, Levinovitz A, Khademi M, Olsson T. Expression of MHC class I and beta2-microglobulin in rat spinal motoneurons: regulatory influences by IFN-gamma and axotomy. Exp Neurol 1998; 150: 282–95.

Liu X, Milo M, Lawrence ND, Rattray M. Probe-level measurement error improves accuracy in detecting differential gene expression. Bioinformatics 2006; 22: 2107–13.

Lo KW, Kogoy JM, Pfister KK. The DYNLT3 light chain directly links cytoplasmic dynein to a spindle checkpoint protein, Bub3. J Biol Chem 2007; 282: 11205–12.

Lobsiger CS, Boillée S, Cleveland DW. Toxicity from different SOD1 mutants dysregulates the complement system and the neuronal regenerative response in ALS motor neurons. Proc Natl Acad Sci USA 2007; 104: 7319–26.

Lobsiger CS, Cleveland DW. Glial cells as intrinsic components of non-cellautonomous neurodegenerative disease. Nat Neurosci 2007; 10: 1355–60.

Longatti A, Tooze SA. Vesicular trafficking and autophagosome formation. Cell Death Differ 2009; 16: 956–65.

Magrané J, Manfredi G. Mitochondrial function, morphology, and axonal transport in amyotrophic lateral sclerosis. Antioxid Redox Signal 2009; 11: 1615–26.

Maier M, Peng Y, Jiang L, Seabrook TJ, Carroll MC, Lemere CA. Complement C3 deficiency leads to accelerated amyloid beta plaque deposition and neurodegeneration and modulation of the microglia/macrophage phenotype in amyloid precursor protein transgenic mice. J Neurosci 2008; 28: 6333–41.

Mancuso R, Oliván S, Mancera P, Pastén-Zamorano A, Manzano R, Casas C, et al. Effect of genetic background on onset and disease progression in the SOD1-G93A model of amyotrophic lateral sclerosis. Amyotroph Lateral Scler 2012; 13: 302–10.

Maragakis NJ, Rothstein JD. Mechanisms of disease: astrocytes in neurodegenerative disease. Nat Clin Pract Neurol 2006; 2: 679–89.

Martinez-Arca S, Coco S, Mainguy G, Schenk U, Alberts P, Bouillé P, et al. A common exocytotic mechanism mediates axonal and dendritic outgrowth. J Neurosci 2001; 21: 3830–8.

Mead RJ, Higginbottom A, Bennett E, Kirby J, Barber SC, Allen SP, et al. Pharmacological NRF2-ARE pathway activation is protective in mouse and patient fibroblast models of amyotrophic lateral sclerosis. Free Radic Biol Med 2013; 61C: 438–452.

Medana I, Martinic MA, Wekerle H, Neumann H. Transection of major histocompatibility complex class I-induced neurites by cytotoxic T lymphocytes. Am J Pathol 2001; 159: 809–15.

Miller KE, Sheetz MP. Axonal mitochondrial transport and potential are correlated. J Cell Sci 2004; 117: 2791–804.

Millecamps S, Julien JP. Axonal transport deficits and neurodegenerative diseases. Nat Rev Neurosci 2013; 14: 161–76.

Mills EM, Xu D, Fergusson MM, Combs CA, Xu Y, Finkel T. Regulation of cellular oncosis by uncoupling protein 2. J Biol Chem 2002; 277: 27385–92.

Muchamuel T, Basler M, Aujay MA, Suzuki E, Kalim KW, Lauer C, et al. A selective inhibitor of the immunoproteasome subunit LMP7 blocks cytokine production and attenuates progression of experimental arthritis. Nat Med 2009; 15: 781–7.

Mukherjee P, Pasinetti GM. Complement anaphylatoxin C5a neuroprotects through mitogen-activated protein kinase-dependent inhibition of caspase 3. J Neurochem 2001; 77: 43–9.

Mukherjee P, Thomas S, Pasinetti GM. Complement anaphylatoxin C5a neuroprotects through regulation of glutamate receptor subunit 2 in vitro and in vivo. J Neuroinflammation 2008; 5: 5.

Nagata T, Nagano I, Shiote M, Narai H, Murakami T, Hayashi T, et al. Elevation of MCP-1 and MCP-1/VEGF ratio in cerebrospinal fluid of amyotrophic lateral sclerosis patients. Neurol Res 2007; 29: 772–6.

Nakayama A, Odajima T, Murakami H, Mori N, Takahashi M. Characterization of two promoters that regulate alternative transcripts in the microtubule-associated protein (MAP) 1A gene. Biochim Biophys Acta 2001; 1518: 260–6.

Nardo G, Pozzi S, Mantovani S, Garbelli S, Marinou K, Basso M, et al. Nitroproteomics of peripheral blood mononuclear cells from patients and a rat model of ALS. Antioxid Redox Signal 2009; 11: 1559–67.

Nardo G, Pozzi S, Pignataro M, Lauranzano E, Spano G, Garbelli S, et al. Amyotrophic lateral sclerosis multiprotein biomarkers in peripheral blood mononuclear cells. PLoS One 2011; 6: e25545.

Nickerson DP, West M, Odorizzi G. Did2 coordinates Vps4-mediated dissociation of ESCRT-III from endosomes. J Cell Biol 2006; 175: 715–20.

O'Barr SA, Caguioa J, Gruol D, Perkins G, Ember JA, Hugli T, et al. Neuronal expression of a functional receptor for the C5a complement activation fragment. J Immunol 2001; 166: 4154–62.

Oliveira AL, Thams S, Lidman O, Piehl F, Hökfelt T, Kärre K, et al. A role for MHC class I molecules in synaptic plasticity and regeneration of neurons after axotomy. Proc Natl Acad Sci USA 2004; 101: 17843–8.

Osaka H, Mukherjee P, Aisen PS, Pasinetti GM. Complement-derived anaphylatoxin C5a protects against glutamate-mediated neurotoxicity. J Cell Biochem 1999; 73: 303–11.

Palmer KJ, Hughes H, Stephens DJ. Specificity of cytoplasmic dynein subunits in discrete membrane-trafficking steps. Mol Biol Cell 2009; 20: 2885–99.

Papadimitriou D, Le Verche V, Jacquier A, Ikiz B, Przedborski S, Re DB. Inflammation in ALS and SMA: sorting out the good from the evil. Neurobiol Dis 2010; 37: 493–502.

Parkinson N, Ince PG, Smith MO, Highley R, Skibinski G, Andersen PM, et al. ALS phenotypes with mutations in CHMP2B (charged multivesicular body protein 2B). MRC Proteomics in ALS Study; FReJA Consortium. Neurology 2006; 67: 1074–7.

Pearson RD, Liu X, Sanguinetti G, Milo M, Lawrence ND, Rattray M. puma: a Bioconductor package for propagating uncertainty in microarray analysis. BMC Bioinformatics 2009; 10: 211.

Perrin FE, Boisset G, Docquier M, Schaad O, Descombes P, Kato AC. No widespread induction of cell death genes occurs in pure motoneurons in an amyotrophic lateral sclerosis mouse model. Hum Mol Genet 2005; 14: 3309–20.

Perrin FE, Boisset G, Lathuilière A, Kato AC. Cell death pathways differ in several mouse models with motoneurone disease: analysis of pure motoneurone populations at a presymptomatic age. Neurochem 2006; 98: 1959–72.

Peviani M, Caron I, Pizzasegola C, Gensano F, Tortarolo M, Bendotti C. Unraveling the complexity of amyotrophic lateral sclerosis: recent advances from the transgenic mutant SOD1 mice. CNS Neurol Disord Drug Targets 2010; 9: 491–503.

Pickering AM, Koop AL, Teoh CY, Ermak G, Grune T, Davies KJ. The immunoproteasome, the 20S proteasome and the PA28$\alpha\beta$ proteasome regulator are oxidative-stress-adaptive proteolytic complexes. Biochem J 2010; 432: 585–94.

Pickering AM, Linder RA, Zhang H, Forman HJ, Davies KJ. Nrf2-dependent induction of proteasome and Pa28$\alpha\beta$ regulator are required for adaptation to oxidative stress. J Biol Chem 2012; 287: 10021–31.

Pizzasegola C, Caron I, Daleno C, Ronchi A, Minoia C, Carrì MT, et al. Treatment with lithium carbonate does not improve disease progression in two different strains of SOD1 mutant mice. Amyotroph Lateral Scler 2009; 10: 221–8.

Qiu XB, Ouyang SY, Li CJ, Miao S, Wang L, Goldberg AL. hRpn13/ADRM1/GP110 is a novel proteasome subunit that binds the deubiquitinating enzyme, UCH37. EMBO J 2006; 25: 5742–53.

Rattray M, Liu X, Sanguinetti G, Milo M, Lawrence ND. Propagating uncertainty in microarray data analysis. Brief Bioinform 2006; 7: 37–47.

Regnard C, Fesquet D, Janke C, Boucher D, Desbruyéres E, Koulakoff A, et al. Characterisation of PGs1, a subunit of a protein complex co-purifying with tubulin polyglutamylase. J Cell Sci 2003; 116: 4181–90.

Robberecht W, Philips T. The changing scene of amyotrophic lateral sclerosis. Nat Rev Neurosci 2013; 14: 248–64.

Rus H, Cudrici C, Niculescu F. The role of the complement system in innate immunity. Immunol Res 2005; 33: 103–12.
Sann S, Wang Z, Brown H, Jin Y. Roles of endosomal trafficking in neurite outgrowth and guidance. Trends Cell Biol 2009; 19: 317–24.
Santos MS, Li H, Voglmaier SM. Synaptic vesicle protein trafficking at the glutamate synapse. Neuroscience 2009; 158: 189–203.
Sarafi MN, Garcia-Zepeda EA, MacLean JA, Charo IF, Luster AD. Murine monocyte chemoattractant protein (MCP)-5: a novel CC chemokine that is a structural and functional homologue of human MCP-1. J Exp Med 1997; 185: 99–109.
Sarlette A, Krampfl K, Grothe C, Neuhoff N, Dengler R, Petri S. Nuclear erythroid 2-related factor 2 antioxidative response element signaling pathway in motor cortex and spinal cord in amyotrophic lateral sclerosis. J Neuropathol Exp Neurol 2008; 67: 1055–1062.
Saro D, Li T, Rupasinghe C, Paredes A, Caspers N, Spaller MR. A thermodynamic ligand binding study of the third PDZ domain (PDZ3) from the mammalian neuronal protein PSD-95. Biochemistry 2007; 46: 6340–52.
Saxena S, Cabuy E, Caroni P. A role for motoneuron subtype-selective ER stress in disease manifestations of FALS mice. Nat Neurosci 2009; 12: 627–36.
Schmitt-John T, Drepper C, Mussmann A, Hahn P, Kuhlmann M, Thiel C, et al. Mutation of Vps54 causes motor neuron disease and defective spermiogenesis in the wobbler mouse. Nat Genet 2005; 37: 1213–5.
Sebastià J, Kieran D, Breen B, King MA, Netteland DF, Joyce D, et al. Angiogenin protects motoneurons against hypoxic injury. Cell Death Differ 2009; 16: 1238–47.
Senaldi G, Varnum BC, Sarmiento U, Starnes C, Lile J, Scully S, et al. Novel neurotrophin-1/B cell-stimulating factor-3: a cytokine of the IL-6 family. Proc Natl Acad Sci USA 1999; 96: 11458–63.
Serviddio G, Bellanti F, Tamborra R, Rollo T, Capitanio N, Romano AD, et al. Uncoupling protein-2 (UCP2) induces mitochondrial proton leak and increases susceptibility of non-alcoholic steatohepatitis (NASH) liver to ischaemia-reperfusion injury. Gut 2008; 57: 957–65.
Shatz CJ. MHC class I: an unexpected role in neuronal plasticity. Neuron 2009; 64: 40–5.
Shi P, Gal J, Kwinter DM, Liu X, Zhu H. Mitochondrial dysfunction in amyotrophic lateral sclerosis. Biochim Biophys Acta 2010; 1802: 45–51.
Shih AY, Johnson DA, Wong G, Kraft AD, Jiang L, Erb H, et al. Coordinate regulation of glutathione biosynthesis and release by Nrf2-expressing glia potently protects neurons from oxidative stress. J Neurosci 2003; 23: 3394–406.
Shinjyo N, Ståhlberg A, Dragunow M, Pekny M, Pekna M. Complement-derived anaphylatoxin C3a regulates in vitro differentiation and migration of neural progenitor cells. Stem Cells 2009; 27: 2824–32.
Skibinski G, Parkinson NJ, Brown JM, Chakrabarti L, Lloyd SL, Hummerich H, et al. Mutations in the endosomal ESCRTIII-complex subunit CHMP2B in frontotemporal dementia. Nat Genet 2005; 37: 806–8.
Skorupa A, King MA, Aparicio IM, Dussmann H, Coughlan K, Breen B, et al. Motoneurons secrete angiogenin to induce RNA cleavage in astroglia. J Neurosci 2012; 32: 5024–38.
Storey JD. The positive false discovery rate: a Bayesian interpretation and the q-value. Ann Statist 2006; 31: 2013–35.
Tanaka M, Kikuchi H, Ishizu T, Minohara M, Osoegawa M, Motomura K, et al. Intrathecal upregulation of granulocyte colony stimulating factor and its neuroprotective actions on motor neurons in amyotrophic lateral sclerosis. J Neuropathol Exp Neurol 2006; 65: 816–25.
Tararuk T, Ostman N, Li W, Björkblom B, Padzik A, Zdrojewska J, et al. JNK1 phosphorylation of SCG10 determines microtubule dynamics and axodendritic length. J Cell Biol 2006; 173: 265–77.
Taylor AM, Berchtold NC, Perreau VM, Tu CH, Li Jeon N, Cotman CW. Axonal mRNA in uninjured and regenerating cortical mammalian axons. J Neurosci 2009; 29: 4697–707.
Teuling E, Ahmed S, Haasdijk E, Demmers J, Steinmetz MO, Akhmanova A, et al. Motor neuron disease-associated mutant vesicle-associated membrane protein-associated protein (VAP) B recruits wild-type VAPs into endoplasmic reticulum-derived tubular aggregates. J Neurosci 2007; 27: 9801–15.
Thams S, Brodin P, Plantman S, Saxelin R, Kärre K, Cullheim S. Classical major histocompatibility complex class I molecules in motoneurons: new actors at the neuromuscular junction. J Neurosci 2009; 29: 13503–15.
Thomas A, Gasque P, Vaudry D, Gonzalez B, Fontaine M. Expression of a complete and functional complement system by human neuronal cells in vitro. Int Immunol 2000; 12: 1015–23.
Tiwari JL, Terasaki PI. HLA and disease associations. New York: Springer-Verlag; 1985.
Tocco G, Musleh W, Sakhi S, Schreiber SS, Baudry M, Pasinetti GM. Complement and glutamate neurotoxicity. Genotypic influences of C5 in a mouse model of hippocampal neurodegeneration. Mol Chem Neuropathol 1997; 31: 289–300.
Tong L, Smyth D, Kerr C, Catterall J, Richards CD. Mitogen-activated protein kinases Erk1/2 and p38 are required for maximal regulation of TIMP-1 by oncostatin M in murine fibroblasts. Cell Signal 2004; 16: 1123–32.
Tsujino H, Kondo E, Fukuoka T, Dai Y, Tokunaga A, Miki K, et al. Activating transcription factor 3 (ATF3) induction by axotomy in sensory and motoneurons: a novel neuronal marker of nerve injury. Mol Cell Neurosci 2000; 15: 170–82.
Turner BJ, Talbot K. Transgenics, toxicity and therapeutics in rodent models of mutant SOD1-mediated familial ALS. Prog Neurobiol 2008; 85: 94–134.
Van Beek J, Nicole O, Ali C, Ischenko A, MacKenzie ET, Buisson A, et al. Complement anaphylatoxin C3a is selectively protective against NMDA-induced neuronal cell death. Neuroreport 2001; 12: 289–93.
Van Hoecke A, Schoonaert L, Lemmens R, Timmers M, Staats KA, Laird AS, et al. EPHA4 is a disease modifier of amyotrophic lateral sclerosis in animal models and in humans. Nat Med 2012; 18: 1418–22.
Vargas MR, Johnson DA, Sirkis DW, Messing A, Johnson JA. Nrf2 activation in astrocytes protects against neurodegeneration in mouse models of familial amyotrophic lateral sclerosis. J Neurosci 2008; 28: 13574–81.
Vlug AS, Teuling E, Haasdijk ED, French P, Hoogenraad CC, Jaarsma D. ATF3 expression precedes death of spinal motoneurons in amyotrophic lateral sclerosis-SOD1 transgenic mice and correlates with c-Jun phosphorylation, CHOP expression, somato-dendritic ubiquitination and Golgi fragmentation. Eur J Neurosci 2005; 22: 1881–94.
Wahl AF, Wallace PM. Oncostatin M in the anti-inflammatory response. Ann Rheum Dis 2001; 60 (Suppl 3): iii75–80.
Wallimann T, Wyss M, Brdiczka D, Nicolay K, Eppenberger HM. Intracellular compartmentation, structure and function of creatine kinase isoenzymes in tissues with high and fluctuating energy demands: the 'phosphocreatine circuit' for cellular energy homeostasis. Biochem J 1992; 281: 21–40.
Wallace PM, MacMaster JF, Rouleau KA, Brown TJ, Loy JK, Donaldson KL, et al. Regulation of inflammatory responses by oncostatin M. J Immunol 1999; 162: 5547–55. Erratum in: J Immunol 2000; 164: 5531.
Weiss TW, Kvakan H, Kaun C, Zorn G, Speidl WS, Pfaffenberger S, et al. The gp130 ligand oncostatin M regulates tissue inhibitor of metalloproteinases-1 through ERK1/2 and p38 in human adult cardiac myocytes and in human adult cardiac fibroblasts: a possible role for the gp130/gp130 ligand system in the modulation of extracellular matrix degradation in the human heart. J Mol Cell Cardiol 2005; 39: 545–551.
Weiss TW, Samson AL, Niego B, Daniel PB, Medcalf RL. Oncostatin M is a neuroprotective cytokine that inhibits excitotoxic injury in vitro and in vivo. FASEB J 2006; 20: 2369–71.
Xia CH, Roberts EA, Her LS, Liu X, Williams DS, Cleveland DW, Goldstein LS. Abnormal neurofilament transport caused by targeted

disruption of neuronal kinesin heavy chain KIF5A. J Cell Biol 2003; 161: 55–66.

Yamanak K, Chun SJ, Boillee S, Fujimori-Tonou N, Yamashita H, Gutmann DH, et al. Astrocytes as determinants of disease progression in inherited amyotrophic lateral sclerosis. Nat Neurosci 2008; 11: 251–3.

Yanamadala V, Friedlander RM. Complement in neuroprotection and neurodegeneration. Trends Mol Med 2010; 16: 69–76.

Yao T, Song L, Xu W, DeMartino GN, Florens L, Swanson SK, et al. Proteasome recruitment and activation of the Uch37 deubiquitinating enzyme by Adrm1. Nat Cell Biol 2006; 8: 994–1002.

Yepes M, Sandkvist M, Wong MK, Coleman TA, Smith E, Cohan SL, et al. Neuroserpin reduces cerebral infarct volume and protects neurons from ischemia-induced apoptosis. Blood 2000; 96: 569–76.

Yi FH, Lautrette C, Vermot-Desroches C, Bordessoule D, Couratier P, Wijdenes J, et al. In vitro induction of neuronal apoptosis by anti-Fas antibody-containing sera from amyotrophic lateral sclerosis patients. J Neuroimmunol 2000; 109: 211–20.

Yu JX, Bradt BM, Cooper NR. Constitutive expression of proinflammatory complement components by subsets of neurons in the central nervous system. J Neuroimmunol 2002; 123: 91–101.

Zacchigna S, Lambrechts D, Carmeliet P. Neurovascular signalling defects in neurodegeneration. Nat Rev Neurosci 2008; 9: 169–81.

Zerial M, McBride H. Rab proteins as membrane organizers. Nat Rev Mol Cell Biol 2001; 2: 107–17.

Zhong Z, Deane R, Ali Z, Parisi M, Shapovalov Y, O'Banion MK, et al. ALS-causing SOD1 mutants generate vascular changes prior to motor neuron degeneration. Nat Neurosci 2008; 11: 420–2.